Mechanism of activation of an ancestral Tec kinase by PIP_3

Eva Krötenheerdt[1,2], Freia von Raußendorf[1], Ronja Reinhardt[1], Lucas Piëch[1,2], Nicholas Wedige[3], Hunter G. Nyvall[4], John E. Burke[4,5] and Thomas A. Leonard[1,*]

[1]Max Perutz Labs, Medical University of Vienna, Dr. Bohr-Gasse 9, 1030, Vienna, Austria

[2]Vienna BioCenter PhD Program, a Doctoral School of the University of Vienna and the Medical University of Vienna, A-1030 Vienna, Austria

[3]BioOptics Light Microscopy Facility, Max Perutz Labs, Dr. Bohr-Gasse 9, 1030 Vienna, Austria

[4]Department of Biochemistry and Microbiology, University of Victoria, Victoria, BC, Canada V8W 2Y2

[5]Department of Biochemistry and Molecular Biology, University of British Columbia, Vancouver, British Columbia V6T 1Z3, Canada

[*]Correspondence: thomas.leonard@meduniwien.ac.at

Abstract

The Tec kinases are a family of five paralogous mammalian genes that play crucial roles in cell growth, proliferation and differentiation, particularly in immune cells. The recruitment and activation of the Tec kinases depends on the generation of the lipid second messenger, PIP_3, in the plasma membrane. However, the mechanisms by which PIP_3 activates the Tec kinases are not well understood. In order to elucidate the mechanism by which all Tec kinases are regulated by PIP_3, we studied an ancestral Tec kinase from the choanoflagellate *Monosiga brevicollis.* Here, we demonstrate that PIP_3 relieves autoinhibition of MbTec by displacing its PH domain from an inhibitory interaction with its kinase domain. Unexpectedly, we found that a conserved polyproline motif within MbTec promotes its activation in a kinase-intrinsic mechanism. Finally, we show that the PH domain is sufficient to restore autoinhibition in a constitutively active mutant of MbTec. Our findings reveal that PIP_3 is necessary, but not sufficient for MbTec activation and that the coincident detection of multiple membrane-localized signals is required to switch MbTec on.

Introduction

The Tec kinases are a subfamily of the Src family of non-receptor tyrosine kinases (SFK), best known for their roles in the proliferation and differentiation of immune cells (1). Of the five mammalian paralogs, mutations in Bruton's tyrosine kinase (BTK) are associated with X-linked agammaglobulinemia (XLA), a disease characterized by a failure of pre-B cells to mature into terminally differentiated, antibody producing B cells and a consequent lack of circulating antibodies (2). Mutations in the same gene lead to X-linked immunodeficiency (XID) in mice (3). Conversely, inhibition of BTK is used in the clinic to treat a range of B cell malignancies, including chronic lymphocytic leukemia (CLL), mantle cell lymphoma, and Waldenström's macroglobulinemia (4).

The Tec kinases are distinguished by an N-terminal pleckstrin homology (PH) domain, which is appended to an ancient Src homology 3 (SH3)- Src homology 2(SH2)-kinase (32K) module shared by all SFKs (5). BTK is autoregulated by its SH3 and SH2 domains, which pack against the kinase domain to maintain it in an inactive conformation (6, 7), as also observed for the SFKs SRC, hematopoietic cell kinase (HCK) and Abelson murine leukemia viral oncogene homolog 1 (ABL) (8–10). The SH3 and SH2 domains bind to phosphorylated tyrosine marks and polyproline motifs in activated receptors at the plasma membrane, respectively. This leads to the specific recruitment of BTK to membrane proximal sites, which is a prerequisite for its activation and subsequent downstream substrate phosphorylation. Early reports suggested that the activation loops of BTK and inducible T-cell kinase (ITK) are *trans*-phosphorylated by SFKs (11–13), while more recent reports have attributed activation loop phosphorylation to autocatalysis (6, 7, 14).

Unlike other SFKs, which are localized to the plasma membrane via myristoylation of their N-termini (15), the localization of the Tec kinases depends on the lipid second messenger phosphatidylinositol-3,4,5-trisphosphate (PIP_3). PIP_3 produced by class I phosphatidylinositol 3-kinases (PI3K) immediately downstream of the B cell receptor (BCR) or T cell receptor (TCR) is required for re-localization of BTK and ITK, respectively, from the cytosol to the plasma membrane. Various functions have been ascribed to the PH domains of BTK and ITK, from targeting to the plasma membrane (16–18) to PIP_3-mediated dimerization (6, 14, 19) and autoinhibition of kinase activity (6, 7, 20, 21). While membrane targeting and co-localization of ITK with the TCR can be

substituted with the membrane-targeting myristoylation sequence of LCK, the PH domain is indispensable for kinase activation (22). Although full-length BTK has recently been crystallized, the PH domain was not resolved in the electron density map (7), while studies of BTK in solution and by cryo-electron microscopy have concluded that the protein adopts a spectrum of conformations with varying degrees of compaction (7, 23, 24). The role, therefore, of the PH domain in regulating the activity of the Tec kinases is still poorly understood.

The Tec kinases first emerged in unicellular choanoflagellates, before gene duplication, prior to the evolution of vertebrates, gave rise to the five mammalian paralogs (25). Tissue-specific expression patterns, particularly in immune cells, have since given rise to the diversification of the signaling pathways regulated by individual paralogs (26). In order to elucidate the mechanism by which all Tec kinases are regulated by PIP_3, we studied an ancestral Tec kinase from the choanoflagellate *Monosiga brevicollis*, which we hereinafter refer to as MbTec. We show that MbTec adopts a well-defined, compact conformation in solution and that the PH domain both stabilizes this conformation and inhibits its kinase activity. We provide evidence that the PIP_3-binding pocket of the PH domain is sequestered in an autoinhibitory conformation centered on the kinase domain of MbTec and that a previously reported gain-of-function mutation in the PH domain of BTK activates MbTec independently of PIP_3. Finally, we demonstrate that a conserved polyproline motif in MbTec plays a crucial role in its allosteric, PIP_3-mediated activation. Our findings reveal that activation of MbTec is explicitly dependent on PIP_3, thereby confining its activity to the membrane. Tec kinases are, therefore, coincident detectors of PIP_3, phospho-tyrosine and polyproline motifs, all of which must be engaged in order to switch Tec on.

Results

Monosiga brevicollis Tec binds and is stabilized by ADP

MbTec is a 667 amino acid long protein with 42% sequence identity to human BTK. It comprises a PH domain at its N-terminus followed immediately by a Tec homology (TH) domain, an unstructured linker of approximately 85 amino acids that contains a conserved polyproline motif, SH3, SH2 and kinase domains (Figure 1A). The TH domain is not, in fact, an independently folding domain, but a zinc finger that is an intrinsic part of the PH domain fold (16). A conserved hydrophobic amino acid in the SH2-kinase linker (MbTec L396) forms the central component of a three-residue hydrophobic stack that serves to maintain the SH3-SH2-kinase module of SFKs in an inactive conformation stabilized by ADP (27). Mutation of the central residue in the hydrophobic stack (Figure 1B-C) is sufficient to convert both SRC and ITK into an active conformation, concomitant with the binding of ATP (27). MbTec Y559 in the activation loop corresponds to the canonical autophosphorylation site (human BTK Y551).

To study the properties of MbTec, we purified wild-type and mutant variants of the full-length protein as well as its isolated PH domain and 32K modules (Figure 1A) to homogeneity. All kinase domain-containing constructs were dephosphorylated *in vitro* with the tyrosine phosphatase YopH and the serine/threonine lambda phosphatase after affinity purification, prior to ion exchange and size-exclusion chromatography. The mass and polydispersity of all purified proteins employed in this study were confirmed by mass spectrometry (Supplementary Figure 1A-K) and mass photometry (Supplementary Figure 2A-K) or size-exclusion chromatography coupled to multi-angle light scattering (SEC-MALS) (Supplementary Figure 2C). To investigate the nucleotide dependence of MbTec, we measured its thermal stability in the presence of ADP, ATP, and a non-hydrolyzable ATP analog, AMPPNP. MbTec was preferentially stabilized by ADP (Figure 1D), consistent with what has previously been observed for SRC and ITK (27).

Advances in computational modeling have made the determination of proteins of unknown structure routine (28), including, recently, the docking of ligands and ions (29). To assess the structure of Tec kinases in silico, we modeled both MbTec and human Btk together with ADP.Mg^{2+} and a single Zn^{2+} ion, which has been observed in the experimentally determined structure of the PH domain (16) using AlphaFold (29). The

five Btk structures and two out of five MbTec structures exhibit a conserved 32K architecture superimposable with the crystal structure of the 32K module of human Btk (6) and the ADP-bound conformation of Src (27). All seven predictions capture the inactive conformation of the activation loop tyrosine, which is sequestered in a non-phosphorylatable position. However, AlphaFold fails to detect any interface with the PH domain (Figure 1E). This raises the question of whether the PH domain exerts any influence on the kinase activity of MbTec.

MbTec is autoinhibited by its PH domain

Previous studies of BTK and ITK have proposed that the PH domain helps maintain the kinase domain in an inactive conformation. However, conflicting data from multiple structural studies, each of which has proposed a different position of the PH domain (6, 7, 23, 24), has made it impossible to unambiguously determine its mechanism of autoinhibition. Furthermore, direct activation of kinase activity by PIP_3 has, as yet, not been demonstrated.

To determine whether the PH domain exerts an autoinhibitory effect on MbTec, we compared the rates of autophosphorylation of $MbTec^{FL}$, $MbTec^{FL}$ L396A, $MbTec^{32K}$ and $MbTec^{32K}$ L396A using a radiometric kinase assay (Figure 2A). $MbTec^{FL}$ exhibited the lowest rate of autophosphorylation, which was only modestly increased by either deletion of the PH domain or mutation of L396 in the SH2-kinase linker, a mutation known to promote the constitutive activation of ITK (27). Combining deletion of the PH domain with mutation of L396, however, increased the rate of autophosphorylation more than 10-fold (Figure 2A). These observations indicate that the PH domain exerts a strong autoinhibitory influence on kinase activity that cannot be overcome by disruption of the SH3-kinase interaction.

To confirm the stoichiometry of autophosphorylation of MbTec, we measured the mass of $MbTec^{FL}$ L396A and $MbTec^{32K}$ L396A post-autophosphorylation by mass spectrometry. We analyzed samples in the linear kinetics regime to capture the most specific events. The increase in mass corresponded to modification with a single phosphate in 40% of $MbTec^{32K}$ L396A molecules under the conditions of the assay (Figure 2B). This correlated well with the calibrated stoichiometry of phosphorylation determined by radiometric kinase assay in Figure 2A. By contrast, $MbTec^{FL}$ L396A

exhibited negligible autophosphorylation (Supplementary Figure 3A), consistent with robust autoinhibition by its PH domain. To identify the modified residue, MbTec^{32K} L396A and MbTec^{FL} L396A were subjected to tandem mass spectrometry, which revealed phosphorylation of the canonical activation loop tyrosine Y559 in MbTec^{32K} L396A, but not MbTec^{FL} L396A (Supplementary Figure 3B). This confirmed that the PH domain specifically inhibits activation loop phosphorylation of MbTec.

Finally, we observed that phosphorylation of a consensus substrate peptide is also robustly activated by the additive effects of both PH and SH3 domain displacement (Figure 2C). Together, these observations indicate that MbTec is robustly autoinhibited by its PH domain, and that PH domain displacement is necessary, but not sufficient, for its activation.

MbTec adopts a compact conformation in solution

Autoinhibition by the PH domain should be manifested in the structure of MbTec. To characterize the size, shape and conformation of MbTec in solution, we employed small-angle X-ray scattering (SAXS). Prior to SAXS data collection, mass photometry revealed that MbTec^{FL}, MbTec^{FL} L396A, MbTec^{32K}, and MbTec^{32K} L396A all exhibit masses consistent with them being monomeric in solution (Supplementary Figure 2A,B,D,E), while SEC-MALS revealed the same for the PH domain (Supplementary Figure 2C). Due to the small size of the PH domain (20 kDa), a reliable mass cannot be obtained by mass photometry. All constructs were observed to be monodisperse.

SAXS data were collected by measuring the scattering of MbTec particles flowing through a quartz capillary immediately downstream of a size exclusion column. Frames were averaged across the elution peak and reduced to a 1D scattering curve (Figure 3A), from which the radius of gyration (R_g) could be estimated by Guinier analysis. The size of globular proteins can be estimated from the slope of the Guinier fit in the low scattering regime and its linearity is a strong indication of particle monodispersity. The plots for MbTec^{FL} and MbTec^{32K} are both linear within the limits of the Guinier approximation (Supplementary Figure 4A-B), indicating that the radius of gyration is well estimated in each case. The raw scattering curves for MbTec^{FL} and MbTec^{32K} were converted into pair distribution functions by Fourier transformation (Figure 3B), from which the radius of gyration and the maximum dimension of each particle could be

estimated (Figure 3C). MbTec^{FL} has an R_g of 3.1 nm and a maximum dimension of 8.4 nm compared with 2.5 nm and 8.3 nm for MbTec^{32K}. Estimation of the molecular mass from the scattering is within 2 kDa of the actual mass of the proteins (Figure 3C). Having established that both proteins behave well in solution and that the measured scattering reflects the behavior of individual, non-aggregated particles, we calculated their respective molecular envelopes from the scattering curves, *ab initio*. Iterative rounds of dummy atom modeling were followed by alignment of the resulting models, trimming of outliers, and refinement of the core electron density. Finally, the best fit of the known structure of the 32K module of SRC was obtained by superposition with the final models. Comparison of the molecular envelopes revealed a region of extra electron density in MbTec^{FL} (Figure 3D) compared to MbTec^{32K} (Figure 3E), putatively in the vicinity of the C-lobe of the kinase domain, though the limited resolution of SAXS data means that placement of the missing PH domain into this density is ambiguous. Nevertheless, SAXS analysis unambiguously revealed a compact intramolecular assembly of MbTec, including its PH domain.

To obtain further insights into the intramolecular association of the MbTec PH domain with its SH3, SH2 and kinase domains, we employed hydrogen-deuterium exchange mass spectrometry (HDX-MS). HDX-MS provides peptide-level information on the rate of exchange of backbone amide hydrogens with a deuterated solvent, thereby revealing changes in secondary structure when comparing two species. To investigate the surfaces of MbTec involved in PH domain sequestration, we compared the rates of HDX between MbTec^{FL} and MbTec^{32K} (Figure 3F) and MbTec^{FL} and MbTec^{PH} (Figure 3G). Deletion of the PH domain resulted in significant increases in the rate of HDX throughout the SH3 domain and in the αC helix, activation loop, and αH-αI loop of the kinase domain (Figure 3H). Conversely, deletion of the 32K module resulted in significant increases in HDX in strands β2, β3, β7 and helix αA of the PH domain (Figure 3I). The time course of deuterium incorporation is shown for individual peptides in these regions in Supplementary Figure 4C (MbTec^{FL} vs MbTec^{32K}) and Supplementary Figure 4D (MbTec^{FL} vs MbTec^{PH}), with the full set of deuterium incorporation data shown in the source data. These observations are consistent with an intramolecular association of the PH domain with the 32K module in MbTec.

A gain-of-function mutation in the PH domain activates MbTec

A previously identified gain-of-function mutation in the PH domain of BTK, E41K, has been proposed to activate BTK by enhancing its binding to PIP_3 at the plasma membrane (17, 18, 30) as well as promoting IP_6-mediated dimerization (31). Since other PIP_3-activated kinases, including Akt and PDK1, have been reported to sequester the PIP_3-binding pocket of their PH domains in an intramolecular, autoinhibitory interface with their kinase domains, we investigated whether the same regulatory principle might extend to the Tec kinases.

Particle parameters, HDX exchange rates, and enzymatic activity all indicate an autoinhibitory interface between the PH domain and the kinase domain in MbTec. Consistent with a physical interaction, the thermal stability of $MbTec^{32K}$ ($MbTec^{\Delta PH}$) was 5-6°C lower than $MbTec^{FL}$ (Figure 4A). $MbTec^{FL}$ E41K (equivalent to human BTK E41K) exhibited a significantly increased rate of autophosphorylation in the absence of PIP_3 compared to wild-type $MbTec^{FL}$, equivalent to the rate of autophosphorylation of $MbTec^{32K}$ L396A, indicating that the E41K mutation weakens PH domain-mediated autoinhibition (Figure 4B). The kinetics of $MbTec^{FL}$ E41K autophosphorylation could be further enhanced by introduction of the L396A mutation, simulating SH3 domain release (Figure 4B).

To further investigate whether the PIP_3 binding pocket was part of the autoinhibitory interface, we compared the membrane translocation behavior of co-expressed $MbTec^{FL}$ with $MbTec^{PH}$ within individual cells. $MbTec^{FL}$ exhibited a primarily diffuse cytoplasmic distribution with minor enrichment of $MbTec^{PH}$ at membrane protrusions (Figure 4C). Upon stimulation of the cells with PDGFαβ, $MbTec^{PH}$ exhibited considerably stronger enrichment at membrane protrusions in comparison to $MbTec^{FL}$ (Figure 4C-D, Supplementary Figure 5A). Importantly, while the membrane association of $MbTec^{FL}$ was transient, $MbTec^{PH}$ exhibited prolonged association with the membrane long after $MbTec^{FL}$ had returned to its basal level post-stimulation of the cells with PDGF (Figure 4D, Supplementary Figure 5A). Together, these observations support an autoinhibitory role for the PH domain in which the PIP_3-binding pocket is sequestered in the interface.

We have previously observed that the intramolecular association of the PH and kinase domains of Akt1 is mediated by a loop segment between the activation loop and

helix αF (Figure 4E) (32). The corresponding segment of the Tec kinases exhibits unusually strong conservation in its putatively solvent-exposed surface (Figure 4F), particularly in the residues corresponding to D323 and D325 of Akt1. Since mutation of D323 and D325 in Akt1 to alanine results in a constitutively active, PIP_3-independent kinase due to the loss of PH domain-mediated autoinhibition (33, 34) , we mutated the corresponding residues in MbTec. Comparison of the thermal stability of $MbTec^{32K}$, $MbTec^{FL}$, $MbTec^{FL}$ Y578A R580A and $MbTec^{FL}$ Y578D R580E revealed that whilst ADP stabilizes all four constructs by 2-3°C, deletion of the PH domain reduces the thermal stability of MbTec by 6°C. Mutation of the loop segment reduces the thermal stability by 3-6°C, depending on whether the mutations merely reduce van der Waals contacts (Y578A R580A) or introduce unfavorable interactions (Y578D R580E) (Figure 4G, Supplementary Figure 5B). $MbTec^{FL}$ Y578D R580E exhibited the same thermal stability as $MbTec^{32K}$, indicating that these mutations are sufficient to completely disrupt the PH-kinase interface.

MbTec is allosterically activated by PIP_3

Structurally and biochemically, the evidence presented so far strongly supports the allosteric activation of MbTec by PIP_3. To demonstrate it directly, we employed PIP_3-containing lipid nanodiscs (Figure 5A). We observed that the rate of MbTec autophosphorylation is dramatically enhanced by PIP_3 binding (Figure 5B-C). Mass spectrometry revealed autophosphorylation of up to eight sites in MbTec elicited by PIP_3 (Supplementary Figure 6A), of which five sites correspond to tyrosines in the SH3 and SH2 domains (Supplementary Figure 6B-C), as well as *trans*-phosphorylation of the nanodisc membrane scaffold protein (MSP1) (Supplementary Figure 6D). These observations indicate that additional interactions within the 'signalosome' are likely required for high-fidelity auto- and substrate phosphorylation.

Curiously, an additive effect of PIP_3 binding and displacement of the SH3 domain (L396A) was not manifested in increased kinetics of autophosphorylation (Figure 5B-C), as previously observed when the PH domain was deleted (Figure 2A). This finding suggests that PIP_3 binding elicits complete allosteric activation of $MbTec^{FL}$, which cannot be phenocopied by simple deletion of the PH domain in $MbTec^{32K}$. Previous studies have reported an intramolecular association of the SH3 domain with a conserved polyproline

motif in the PH-SH3 interdomain linker (35–37) (Figure 1A, 5D). A putative intramolecular association of the SH3 domain with this motif upon the allosteric activation of MbTec by PIP_3 is supported by AlphaFold predictions of the interface which converge on near-identical, high confidence models (Figure 5E). These structures are superimposable with experimentally determined structures of the SH3 domain associated with the polyproline motif of both Itk (35) and Tec (36). To test whether the polyproline motif contributes to MbTec activation in the absence of adaptor proteins, we compared the autophosphorylation kinetics of wild-type $MbTec^{FL}$ with $MbTec^{FL}$ bearing a mutated polyproline motif ($MbTec^{FL}$ Gly_6) (Figure 5F). We observed that $MbTec^{FL}$ Gly_6 autophosphorylated considerably slower than $MbTec^{FL}$, suggesting that the polyproline motif plays an active role in MbTec activation. As observed previously, mutation of L396 in the SH2-kinase linker activated MbTec, but addition of the polyproline mutation ($MbTec^{FL}$ Gly_6 L396A) did not have any additive effect. This finding is consistent with the situation in which the polyproline motif can compete with the SH2-kinase linker for binding to the SH3 domain under conditions in which autoinhibition by the PH domain is relieved.

In summary, activation of MbTec is explicitly dependent on PIP_3, which triggers displacement of the PH domain and subsequent engagement of the polyproline linker by the SH3 domain, leading to relief of autoinhibition, autophosphorylation, and downstream substrate phosphorylation.

Discussion

The activation of the Tec kinases has long been known to depend on the disengagement of its SH2 and SH3 regulatory domains upon recruitment to activated receptors and their associated adaptor proteins at the plasma membrane. However, the precise role of the PH domain, beyond targeting to PIP_3-containing membranes, has been more difficult to pin down. Our data reveal a strict dependence on PIP_3 for MbTec activation, consistent with a compact, autoinhibited conformation in which the PH domain is sequestered in an intramolecular interface with the kinase domain.

There are two key takeaways from this study: first, PIP_3 is necessary, but not sufficient for MbTec activation. Binding to a phospho-tyrosine mark and a polyproline motif are also necessary, but not sufficient for activation. MbTec is therefore a coincident detector of three input signals. Given that PIP_3 is generated, and remains, in the plasma membrane, and that phosphorylated tyrosine motifs are locally constrained in the cytoplasmic tails of activated receptors, this spatially confines MbTec signaling to the plasma membrane and temporally confines it to the lifetime of receptor activation. SH3 domain-containing adaptor proteins, such as Grb2, increase the specificity of Tec subcellular localization by binding to polyproline motifs in both Tec and adaptor proteins in the signaling complex. Second, the PH domain is necessary and sufficient to promote autoinhibition of MbTec. Since the PIP_3 binding site of the PH domain is sequestered in the autoinhibited conformation of MbTec, its interaction with PIP_3 is mutually exclusive, which implies a necessary dynamic equilibrium between open and closed conformations of the PH domain that permits sampling of the membrane for PIP_3. Presumably, such a mechanism ensures that autoinhibition is immediately restored as soon as the PIP_3 signal is attenuated by PTEN-mediated dephosphorylation. Similar models have been proposed for the pro-growth and survival kinase Akt (32, 34), phosphoinositide-dependent kinase 1 (PDK1) (38), and serum and glucocorticoid-regulated kinase 3 (SGK3) (39).

What can we conclude, however, about the regulation of mammalian Tec kinases from the study of MbTec? Previous studies have implicated the PH domain in autoinhibition but have disputed the details. On balance, the evidence strongly supports a conserved mechanism of Tec kinase activation by PIP_3. While AlphaFold (28) converges on the known structure of the 32K module of MbTec, the placement of the PH

domain is ambiguous. Equally, the crystal structures of minimal PH-kinase domain constructs of BTK are discrepant (6, 7). Four independent SAXS studies, including this one, have arrived at different conclusions regarding the size and shape of individual particles (7, 23, 24). Importantly, however, mutation of a conserved surface on the kinase domain of MbTec is sufficient to neutralize the stabilizing effect of the PH domain, while mutation of the PH domain surface is sufficient to activate MbTec in the absence of PIP_3. These observations are consistent with previous HDX-MS and NMR spectroscopy of human BTK (20) as well as the inositol hexakisphosphate (IP_6)-mediated activation of bovine BTK in vitro (6). Furthermore, the E41K substitution renders BTK constitutively active in cells (30). E41 is located in close proximity to the PIP_3-binding pocket, which is sequestered in inactive MbTec. Although E41K leads to increased membrane targeting of the BTK PH domain (18, 30), the mutation also promotes BTK activation by relieving PH domain-mediated autoinhibition. Such a mechanism is analogous to a mutation in the PH domain of Akt, E17K, which has been observed in a variety of cancers (41–43), and is causative of the genetic mosaic disorder Proteus Syndrome (44).

We propose the following universal model for the activation of Tec kinases. Activation of cell surface receptors drives phosphorylation of their cytoplasmic tails by non-receptor tyrosine kinases (Figure 6). These phospho-tyrosine marks serve to recruit both the Tec kinase and class I PI3K. Recruitment of Tec alone is insufficient to drive its activation, which depends on the production of PIP_3 by PI3K. Co-localization of autoinhibited Tec and PI3K at the plasma membrane increases the probability that Tec will be activated by PIP_3 upon its production; indeed, XLA-associated mutations of the SH2 domain of BTK, including the phospho-tyrosine coordinating residue, Arg307, inhibit binding to the adaptor protein B-cell linker protein (BLNK) (45, 46) and impair BTK activation in cells (24). The SH2 domain of ITK is similarly required for its activation downstream of the TCR (47). PIP_3-mediated activation of Tec, coincident with the intramolecular engagement of its SH3 domain with its own polyproline ligand, promotes its activation by autophosphorylation, an event that has been proposed to be mediated in *trans* by activation loop exchange and which is supported by dimerization of MbTec on PIP_3-containing membranes (7).

Although our data is insufficient to exclude the possibility that adaptor proteins such as Grb2 (48) directly activate Tec in cells, the high local concentration of the polyproline motif and SH3 domain (intra-Tec) favors a Tec-autonomous model (Figure 6). Indeed, the *cis*-interaction of the polyproline motif in ITK has been shown to prevent the binding of SH3 domain-containing adaptor proteins such as Sam68 and Grb2 (35). In this sense, it is possible that adaptor proteins, such as Grb2, govern the subcellular localization of autoinhibited Tec kinases, whose activation is then accomplished in a PI3K-dependent and Tec-intrinsic manner. Such a model would provide a coincidence-based mechanism for the discrete subcellular localization of Tec kinases with PI3K prior to their activation. Grb2 is localized to the BCR via its SH2 domain upon tyrosine phosphorylation of the immunoglobulin heavy chain (49), while the N-terminal SH3 domain (N-SH3) has been shown to bind to the polyproline motifs of BTK and ITK in vitro (35, 48). The C-terminal SH3 domain (C-SH3) binds to the p85 regulatory subunit of PI3K both *in vitro* and *in vivo* (50). Accordingly, lineage-specific deletion of Grb2 in mice leads to impaired B-cell differentiation and IgG responses (51). A recent study has also proposed that Grb2 could promote BTK activation by binding to the SH2-kinase linker (48), an event that could be promoted by competitive displacement of the polyproline motif from Grb2 by the SH3 domain of Tec upon PIP_3-mediated activation. Taken together, Grb2 could be thought of as an activation chaperone, mediating both the specific subcellular recruitment of inactive BTK as well as stabilizing its PIP_3-activated conformation. Whether the SH3-polyproline interaction within Tec occurs in *cis* (intramolecular) or *trans* (intermolecular) upon PIP_3 binding will require further investigation, though a *trans* interaction would neatly promote dimerization and autophosphorylation. Here, it should be noted that PIP_3-dependent dimerization of the PH domain of BTK, but not those of TEC or ITK, is required for BTK autophosphorylation and downstream signaling in B-cells (6, 14, 19, 52), indicating that paralog-specific evolutionary adaptations likely created additional layers of control over dimerization, kinase activation and, ultimately, signaling specificity.

Upon attenuation of the PIP_3 signal, dissociation of its PH domain from the membrane restores Tec autoinhibition, leading to immediate shutdown of the downstream signaling pathway. The coincident detection of each signal in space and time ensures the propagation of the signal with high fidelity and almost certainly limits the available substrate pool to those substrates co-localized to the site of Tec activation

on the membrane. This is consistent with the membrane localization of one of the best characterized substrates of BTK, phospholipase C (PLC) γ (53, 54). However, more sophisticated reconstitutions with interaction partners will undoubtedly be required to elucidate precisely what is necessary and sufficient for high-fidelity substrate phosphorylation. In conclusion, the Tec kinases are exquisitely tuned detectors that function in much the same way that an AND logic gate works in an electronic circuit.

Acknowledgements

We thank Dr. Adam Round, who assisted in SAXS data collection on beamline BM29 at the ESRF, Grenoble. A plasmid encoding the DNA sequence of MbTec and an expression plasmid for YopH were kind gifts from Dr. Todd Miller (Stony Brook University, NY, USA). This work was supported by the following grants from the Austrian Science Fund to T.A.L.: P28135, P30584, P33066, and P36212. JEB is supported by the Cancer Research Society (operating grant 1052949).

Author Contributions

Proteins were expressed and purified by E.K., F.v.R. and R.R. All samples for SAXS analysis were purified by F.v.R. SAXS data were collected and analyzed by T.A.L. Kinase assays were performed by E.K. and F.v.R. Samples for HDX-MS were purified by E.K. and analyzed by H.G.N. Thermal stability assays were performed by E.K. and F.v.R. L.P. prepared PIP_3-containing lipid nanodiscs. T.A.L. conceived the project. E.K., R.R. and T.A.L. wrote the manuscript. T.A.L. and J.E.B. obtained funding for the work.

Materials and Methods

Thermal stability assays

Differential scanning fluorimetry measurements were performed in SEC buffer with 5x SYPRO Orange (life technologies) using a BioRad iQ5 Multicolor Real-Time PCR detection system. For each sample, the protein was diluted to 0.1 mg/mL either in the presence or absence of 1 mM ADP and 2 mM $MgCl_2$. The samples were heated from 25 °C to 90 °C in increments of 0.5 °C. The melting temperature was determined from the second derivative of the melting curve and averaged from three independent measurements.

Radiometric kinase assay

All radiometric kinase assays were performed using radiolabeled [γ^{32} P] (Hartman Analytic) at room temperature in the same buffer (20 mM HEPES pH 7.4, 150 mM NaCl, 2 % glycerol, 1 mM TCEP, 1 mM ATP and 2 mM $MgCl_2$ spiked with 1:50 [γ^{32} P] ATP) and a final protein concentration of 0.5 - 2 µM. After clarifying the dephosphorylated protein sample, it was incubated for the indicated duration. At each time point a 10 µL sample was collected and the reaction was quenched by adding 2.5 µL of 1 M EDTA and 3 µL 5x SDS Loading Dye. The samples were separated by SDS-PAGE to remove non-incorporated ATP. The gel was washed 3x 5 min with water, dried and exposed to a phosphor screen overnight. The screen was imaged with an Amersham Typhoon imager and the radioactive signal was quantified with ImageJ. The fraction of phosphorylated MbTec protein was calculated from an internal standard, assuming the incorporation of one phosphate per molecule MbTec (verified by intact mass spectrometry).

For kinase assays containing PIP_3 nanodiscs, MbTec was incubated with nanodiscs in a 4-fold excess of protein (assuming a maximum binding stoichiometry of 4:1 MbTec:nanodisc) for 1 h at room temperature prior to the addition of ATP and $MgCl_2$. The final protein concentration was 1 µM.

ADP-Glo kinase assay

Kinase assays were performed using the ADP-Glo kit (Promega) according to the manufacturer's instructions. Kinase reactions contained 500 nM purified kinase, 50 μM SRC substrate (SignalChem #S30-58), and 1 mM ATP in 20 mM Tris pH 7.5, 100 mM NaCl, 1 mM TCEP, 2 mM $MgCl_2$, and 0.05 mg/ml BSA. Reactions were incubated at RT for the specified time and luminescence was measured using a TECAN Infinite F500 plate reader.

Small-angle X-ray scattering (SAXS)

SAXS data for $MbTec^{FL}$ and $MbTec^{32K}$ were collected on BM29 at the ESRF, Grenoble, France using an in-line SEC-SAXS setup. Proteins were applied to a Agilent Bio SEC 300 column equilibrated in 20 mM Tris, pH 7.4, 150 mM NaCl, 1 mM TCEP and 1 % (v/v) glycerol and images were acquired every second for the duration of the size exclusion run. Buffer subtraction was performed by averaging 50 frames either side of the peak. All subsequent data processing steps were performed using the ATSAS data analysis software 3.9.1. The program DATGNOM (55) was used to generate the pair distribution function [P(r)] for each isoform and to determine D_{max} and R_g from the scattering curves [I(q) vs. q] in an automatic, unbiased manner.

References

1. Andreotti, A. H., Joseph, R. E., Conley, J. M., Iwasa, J., and Berg, L. J. (2018) Multidomain Control Over TEC Kinase Activation State Tunes the T Cell Response. *Annu. Rev. Immunol.* **36**, 549–578
2. Vetrie, D., Vořechovský, I., Sideras, P., Holland, J., Davies, A., Flinter, F., Hammarström, L., Kinnon, C., Levinsky, R., Bobrow, M., Smith, C. I. E., and Bentley, D. R. (1993) The gene involved in X-linked agammaglobulinaemia is a member of the src family of protein-tyrosine kinases. *Nature*. **361**, 226–233
3. Rawlings, D. J., Saffran, D. C., Tsukada, S., Largaespada, D. A., Grimaldi, J. C., Cohen, L., Mohr, R. N., Bazan, J. F., Howard, M., and Copeland, N. G. (1993) Mutation of unique region of Bruton's tyrosine kinase in immunodeficient XID mice. *Science*. **261**, 358–361
4. McDonald, C., Xanthopoulos, C., and Kostareli, E. (2021) The role of Bruton's tyrosine kinase in the immune system and disease. *Immunology*. **164**, 722–736
5. Shah, N. H., Amacher, J. F., Nocka, L. M., and Kuriyan, J. (2018) The Src module: an ancient scaffold in the evolution of cytoplasmic tyrosine kinases. *Crit. Rev. Biochem. Mol. Biol.*
6. Wang, Q., Vogan, E. M., Nocka, L. M., Rosen, C. E., Zorn, J. A., Harrison, S. C., and Kuriyan, J. (2015) Autoinhibition of Bruton's tyrosine kinase (Btk) and activation by soluble inositol hexakisphosphate. *Elife*. 10.7554/eLife.06074
7. Lin, D. Y.-W., Kueffer, L. E., Juneja, P., Wales, T. E., Engen, J. R., and Andreotti, A. H. (2024) Conformational heterogeneity of the BTK PHTH domain drives multiple regulatory states. *Elife*. 10.7554/eLife.89489
8. Sicheri, F., Moarefi, I., and Kuriyan, J. (1997) Crystal structure of the Src family tyrosine kinase Hck. *Nature*. **385**, 602–609
9. Xu, W., Harrison, S. C., and Eck, M. J. (1997) Three-dimensional structure of the tyrosine kinase c-Src. *Nature*. **385**, 595–602
10. Nagar, B., Hantschel, O., Young, M. A., Scheffzek, K., Veach, D., Bornmann, W., Clarkson, B., Superti-Furga, G., and Kuriyan, J. (2003) Structural basis for the autoinhibition of c-Abl tyrosine kinase. *Cell*. **112**, 859–871
11. Heyeck, S. D., Wilcox, H. M., Bunnell, S. C., and Berg, L. J. (1997) Lck phosphorylates the activation loop tyrosine of the Itk kinase domain and activates Itk kinase activity. *J. Biol. Chem.* **272**, 25401–25408
12. Wahl, M. I., Fluckiger, A. C., Kato, R. M., Park, H., Witte, O. N., and Rawlings, D. J. (1997) Phosphorylation of two regulatory tyrosine residues in the activation of Bruton's tyrosine kinase via alternative receptors. *Proc. Natl. Acad. Sci. U. S. A.* **94**, 11526–11533
13. Rawlings, D. J., Scharenberg, A. M., Park, H., Wahl, M. I., Lin, S., Kato, R. M., Fluckiger, A. C., Witte, O. N., and Kinet, J. P. (1996) Activation of BTK by a phosphorylation mechanism initiated by SRC family kinases. *Science*. **271**, 822–825
14. Chung, J. K., Nocka, L. M., Decker, A., Wang, Q., Kadlecek, T. A., Weiss, A., Kuriyan, J., and Groves, J. T. (2019) Switch-like activation of Bruton's tyrosine kinase by membrane-mediated dimerization. *Proc. Natl. Acad. Sci. U. S. A.* **116**, 10798–10803

15. Boggon, T. J., and Eck, M. J. (2004) Structure and regulation of Src family kinases. *Oncogene*. **23**, 7918–7927

16. Hyvönen, M., and Saraste, M. (1997) Structure of the PH domain and Btk motif from Bruton's tyrosine kinase: molecular explanations for X-linked agammaglobulinaemia. *EMBO J.* **16**, 3396–3404

17. Baraldi, E., Djinovic Carugo, K., Hyvönen, M., Surdo, P. L., Riley, A. M., Potter, B. V., O'Brien, R., Ladbury, J. E., and Saraste, M. (1999) Structure of the PH domain from Bruton's tyrosine kinase in complex with inositol 1,3,4,5-tetrakisphosphate. *Structure*. **7**, 449–460

18. Várnai, P., Rother, K. I., and Balla, T. (1999) Phosphatidylinositol 3-kinase-dependent membrane association of the Bruton's tyrosine kinase pleckstrin homology domain visualized in single living cells. *J. Biol. Chem.* **274**, 10983–10989

19. Wang, Q., Pechersky, Y., Sagawa, S., Pan, A. C., and Shaw, D. E. (2019) Structural mechanism for Bruton's tyrosine kinase activation at the cell membrane. *Proceedings of the National Academy of Sciences*. **116**, 9390–9399

20. Amatya, N., Wales, T. E., Kwon, A., Yeung, W., Joseph, R. E., Fulton, D. B., Kannan, N., Engen, J. R., and Andreotti, A. H. (2019) Lipid-targeting pleckstrin homology domain turns its autoinhibitory face toward the TEC kinases. *Proceedings of the National Academy of Sciences*. **116**, 21539–21544

21. Devkota, S., Joseph, R. E., Boyken, S. E., Fulton, D. B., and Andreotti, A. H. (2017) An Autoinhibitory Role for the Pleckstrin Homology Domain of Interleukin-2-Inducible Tyrosine Kinase and Its Interplay with Canonical Phospholipid Recognition. *Biochemistry*. **56**, 2938–2949

22. Ching, K. A., Kawakami, Y., Kawakami, T., and Tsoukas, C. D. (1999) Emt/Itk associates with activated TCR complexes: role of the pleckstrin homology domain. *J. Immunol.* **163**, 6006–6013

23. Márquez, J. A., Smith, C. I. E., Petoukhov, M. V., Lo Surdo, P., Mattsson, P. T., Knekt, M., Westlund, A., Scheffzek, K., Saraste, M., and Svergun, D. I. (2003) Conformation of full-length Bruton tyrosine kinase (Btk) from synchrotron X-ray solution scattering. *EMBO J.* **22**, 4616–4624

24. Duarte, D. P., Lamontanara, A. J., La Sala, G., Jeong, S., Sohn, Y.-K., Panjkovich, A., Georgeon, S., Kükenshöner, T., Marcaida, M. J., Pojer, F., De Vivo, M., Svergun, D., Kim, H.-S., Dal Peraro, M., and Hantschel, O. (2020) Btk SH2-kinase interface is critical for allosteric kinase activation and its targeting inhibits B-cell neoplasms. *Nat. Commun.* **11**, 2319

25. Ortutay, C., Nore, B. F., Vihinen, M., and Smith, C. I. E. (2008) Phylogeny of Tec family kinases identification of a premetazoan origin of Btk, Bmx, Itk, Tec, Txk, and the Btk regulator SH3BP5. *Adv. Genet.* **64**, 51–80

26. Tomlinson, M. G., Kane, L. P., Su, J., Kadlecek, T. A., Mollenauer, M. N., and Weiss, A. (2004) Expression and function of Tec, Itk, and Btk in lymphocytes: evidence for a unique role for Tec. *Mol. Cell. Biol.* **24**, 2455–2466

27. von Raußendorf, F., de Ruiter, A., and Leonard, T. A. (2017) A switch in nucleotide affinity governs activation of the Src and Tec family kinases. *Sci. Rep.* **7**, 17405

28. Jumper, J., Evans, R., Pritzel, A., Green, T., Figurnov, M., Ronneberger, O., Tunyasuvunakool, K., Bates, R., Žídek, A., Potapenko, A., Bridgland, A., Meyer, C., Kohl, S. A. A., Ballard, A. J., Cowie, A., Romera-Paredes, B., Nikolov, S., Jain, R., Adler, J., Back, T., Petersen, S., Reiman, D., Clancy, E., Zielinski, M., Steinegger, M., Pacholska, M., Berghammer, T., Bodenstein, S., Silver, D., Vinyals, O., Senior, A. W., Kavukcuoglu, K., Kohli, P., and Hassabis, D. (2021) Highly accurate protein structure prediction with AlphaFold. *Nature*

29. Abramson, J., Adler, J., Dunger, J., Evans, R., Green, T., Pritzel, A., Ronneberger, O., Willmore, L., Ballard, A. J., Bambrick, J., Bodenstein, S. W., Evans, D. A., Hung, C.-C., O'Neill, M., Reiman, D., Tunyasuvunakool, K., Wu, Z., Žemgulytė, A., Arvaniti, E., Beattie, C., Bertolli, O., Bridgland, A., Cherepanov, A., Congreve, M., Cowen-Rivers, A. I., Cowie, A., Figurnov, M., Fuchs, F. B., Gladman, H., Jain, R., Khan, Y. A., Low, C. M. R., Perlin, K., Potapenko, A., Savy, P., Singh, S., Stecula, A., Thillaisundaram, A., Tong, C., Yakneen, S., Zhong, E. D., Zielinski, M., Žídek, A., Bapst, V., Kohli, P., Jaderberg, M., Hassabis, D., and Jumper, J. M. (2024) Accurate structure prediction of biomolecular interactions with AlphaFold 3. *Nature*. **630**, 493–500

30. Li, T., Tsukada, S., Satterthwaite, A., Havlik, M. H., Park, H., Takatsu, K., and Witte, O. N. (1995) Activation of Bruton's tyrosine kinase (BTK) by a point mutation in its pleckstrin homology (PH) domain. *Immunity*. **2**, 451–460

31. Chowdhury, S., Chakraborty, M. P., Roy, S., Dey, B. P., Gangopadhyay, K., and Das, R. (2024) E41K mutation activates Bruton's tyrosine kinase by stabilizing an inositol hexakisphosphate-dependent invisible dimer. *J. Biol. Chem.* **300**, 107535

32. Truebestein, L., Hornegger, H., Anrather, D., Hartl, M., Fleming, K. D., Stariha, J. T. B., Pardon, E., Steyaert, J., Burke, J. E., and Leonard, T. A. (2021) Structure of autoinhibited Akt1 reveals mechanism of PIP3-mediated activation. *Proc. Natl. Acad. Sci. U. S. A.* 10.1073/pnas.2101496118

33. Ebner, M., Lučić, I., Leonard, T. A., and Yudushkin, I. (2017) PI(3,4,5)P3 Engagement Restricts Akt Activity to Cellular Membranes. *Mol. Cell*. **65**, 416-431.e6

34. Lučić, I., Rathinaswamy, M. K., Truebestein, L., Hamelin, D. J., Burke, J. E., and Leonard, T. A. (2018) Conformational sampling of membranes by Akt controls its activation and inactivation. *Proc. Natl. Acad. Sci. U. S. A.* **115**, E3940–E3949

35. Andreotti, A. H., Bunnell, S. C., Feng, S., Berg, L. J., and Schreiber, S. L. (1997) Regulatory intramolecular association in a tyrosine kinase of the Tec family. *Nature*. **385**, 93–97

36. Pursglove, S. E., Mulhern, T. D., Mackay, J. P., Hinds, M. G., and Booker, G. W. (2002) The solution structure and intramolecular associations of the Tec kinase SRC homology 3 domain. *J. Biol. Chem.* **277**, 755–762

37. Patel, H. V., Tzeng, S. R., Liao, C. Y., Chen, S. H., and Cheng, J. W. (1997) SH3 domain of Bruton's tyrosine kinase can bind to proline-rich peptides of TH domain of the kinase and p120cbl. *Proteins*. **29**, 545–552

38. Levina, A., Fleming, K. D., Burke, J. E., and Leonard, T. A. (2022) Activation of the essential kinase PDK1 by phosphoinositide-driven trans-autophosphorylation. *Nat. Commun.* **13**, 1874

39. Pokorny, D., Truebestein, L., Fleming, K. D., Burke, J. E., and Leonard, T. A. (2021) In vitro reconstitution of Sgk3 activation by phosphatidylinositol 3-phosphate. *J. Biol. Chem.* **297**, 100919

40. Carpten, J. D., Faber, A. L., Horn, C., Donoho, G. P., Briggs, S. L., Robbins, C. M., Hostetter, G., Boguslawski, S., Moses, T. Y., Savage, S., Uhlik, M., Lin, A., Du, J., Qian, Y.-W., Zeckner, D. J., Tucker-Kellogg, G., Touchman, J., Patel, K., Mousses, S., Bittner, M., Schevitz, R., Lai, M.-H. T., Blanchard, K. L., and Thomas, J. E. (2007) A transforming mutation in the pleckstrin homology domain of AKT1 in cancer. *Nature*. **448**, 439–444

41. Landgraf, K. E., Pilling, C., and Falke, J. J. (2008) Molecular mechanism of an oncogenic mutation that alters membrane targeting: Glu17Lys modifies the PIP lipid specificity of the AKT1 PH domain. *Biochemistry*. **47**, 12260–12269

42. Sondka, Z., Dhir, N. B., Carvalho-Silva, D., Jupe, S., Madhumita, McLaren, K., Starkey, M., Ward, S., Wilding, J., Ahmed, M., Argasinska, J., Beare, D., Chawla, M. S., Duke, S., Fasanella, I., Neogi, A. G., Haller, S., Hetenyi, B., Hodges, L., Holmes, A., Lyne, R., Maurel, T., Nair, S., Pedro, H., Sangrador-Vegas, A., Schuilenburg, H., Sheard, Z., Yong, S. Y., and Teague, J. (2024) COSMIC: a curated database of somatic variants and clinical data for cancer. *Nucleic Acids Res.* **52**, D1210–D1217

43. Lindhurst, M. J., Sapp, J. C., Teer, J. K., Johnston, J. J., Finn, E. M., Peters, K., Turner, J., Cannons, J. L., Bick, D., Blakemore, L., Blumhorst, C., Brockmann, K., Calder, P., Cherman, N., Deardorff, M. A., Everman, D. B., Golas, G., Greenstein, R. M., Kato, B. M., Keppler-Noreuil, K. M., Kuznetsov, S. A., Miyamoto, R. T., Newman, K., Ng, D., O'Brien, K., Rothenberg, S., Schwartzentruber, D. J., Singhal, V., Tirabosco, R., Upton, J., Wientroub, S., Zackai, E. H., Hoag, K., Whitewood-Neal, T., Robey, P. G., Schwartzberg, P. L., Darling, T. N., Tosi, L. L., Mullikin, J. C., and Biesecker, L. G. (2011) A mosaic activating mutation in AKT1 associated with the Proteus syndrome. *N. Engl. J. Med.* **365**, 611–619

44. Tzeng, S. R., Pai, M. T., Lung, F. D., Wu, C. W., Roller, P. P., Lei, B., Wei, C. J., Tu, S. C., Chen, S. H., Soong, W. J., and Cheng, J. W. (2000) Stability and peptide binding specificity of Btk SH2 domain: molecular basis for X-linked agammaglobulinemia. *Protein Sci.* **9**, 2377–2385

45. Mattsson, P. T., Lappalainen, I., Bäckesjö, C. M., Brockmann, E., Laurén, S., Vihinen, M., and Smith, C. I. (2000) Six X-linked agammaglobulinemia-causing missense mutations in the Src homology 2 domain of Bruton's tyrosine kinase: phosphotyrosine-binding and circular dichroism analysis. *J. Immunol.* **164**, 4170–4177

46. Ching, K. A., Grasis, J. A., Tailor, P., Kawakami, Y., Kawakami, T., and Tsoukas, C. D. (2000) TCR/CD3-Induced activation and binding of Emt/Itk to linker of activated T cell complexes: requirement for the Src homology 2 domain. *J. Immunol.* **165**, 256–262

47. Nocka, L. M., Eisen, T. J., Iavarone, A. T., Groves, J. T., and Kuriyan, J. (2023) Stimulation of the catalytic activity of the tyrosine kinase Btk by the adaptor protein Grb2. *Elife*. 10.7554/eLife.82676

48. Engels, N., König, L. M., Heemann, C., Lutz, J., Tsubata, T., Griep, S., Schrader, V., and Wienands, J. (2009) Recruitment of the cytoplasmic adaptor Grb2 to surface IgG

and IgE provides antigen receptor-intrinsic costimulation to class-switched B cells. *Nat. Immunol.* **10**, 1018–1025

49. Wang, J., Auger, K. R., Jarvis, L., Shi, Y., and Roberts, T. M. (1995) Direct association of Grb2 with the p85 subunit of phosphatidylinositol 3-kinase. *J. Biol. Chem.* **270**, 12774–12780

50. Ackermann, J. A., Radtke, D., Maurberger, A., Winkler, T. H., and Nitschke, L. (2011) Grb2 regulates B-cell maturation, B-cell memory responses and inhibits B-cell Ca2+ signalling: Grb2-deficient mice. *EMBO J.* **30**, 1621–1633

51. Eisen, T. J., Ghaffari-Kashani, S., Hung, C.-L., Groves, J. T., Weiss, A., and Kuriyan, J. (2025) Conditional requirement for dimerization of the membrane-binding module for BTK signaling in lymphocyte cell lines. *Sci. Signal.* 10.1126/scisignal.ado1252

52. Schaeffer, E. M., Debnath, J., Yap, G., McVicar, D., Liao, X. C., Littman, D. R., Sher, A., Varmus, H. E., Lenardo, M. J., and Schwartzberg, P. L. (1999) Requirement for Tec kinases Rlk and Itk in T cell receptor signaling and immunity. *Science.* **284**, 638–641

53. Petro, J. B., and Khan, W. N. (2001) Phospholipase C-gamma 2 couples Bruton's tyrosine kinase to the NF-kappaB signaling pathway in B lymphocytes. *J. Biol. Chem.* **276**, 1715–1719

54. Petoukhov, M. V., Konarev, P. V., Kikhney, A. G., Svergun, D. I., and IUCr (2007) *ATSAS* 2.1 – towards automated and web-supported small-angle scattering data analysis. *J. Appl. Crystallogr.* **40**, s223–s228

55. Manalastas-Cantos, K., Konarev, P. V., Hajizadeh, N. R., Kikhney, A. G., Petoukhov, M. V., Molodenskiy, D. S., Panjkovich, A., Mertens, H. D. T., Gruzinov, A., Borges, C., Jeffries, C. M., Svergun, D. I., and Franke, D. (2021) ATSAS 3.0: expanded functionality and new tools for small-angle scattering data analysis. *J. Appl. Crystallogr.* **54**, 343–355

Figure Legends

Figure 1. *Monosiga brevicollis* Tec binds and is stabilized by ADP.

A. Domain schematics of all protein constructs used in this study.

B. Hydrophobic stack conservation in MbTec.

C. AlphaFold prediction of the hydrophobic stack in MbTec (right panel), compared to the experimentally determined structure of those of Src (left panel) and Btk (middle panel). The middle residue in the stack, contributed by the SH2-kinase linker, is shown in red.

D. Thermal stability measurements of MbTec as a function of nucleotide concentration. ADP (red), ATP (green), AMPPNP (ANP; blue).

E. Five independent AlphaFold predictions of the structure of human Btk. Bottom right: pair alignment error (PAE) plot for model 1.

Figure 2. MbTec is autoinhibited by its PH domain.

A. Radiometric autophosphorylation assays of $MbTec^{FL}$ (black, solid line) and $MbTec^{32K}$ (black, dashed line), as well as their L396A counterparts (red). Right: representative cartoons and autoradiograph for each construct.

B. Mass spectrometry analysis of the product of $MbTec^{32K}$ L396A autophosphorylation (denoted by the black circle in panel A). Intensities before autophosphorylation in black (left axis) and after autophosphorylation in red (right axis).

C. Substrate peptide phosphorylation by $MbTec^{FL}$ (black, solid line), $MbTec^{FL}$ L396A (black, dashed line), $MbTec^{32K}$ (red, solid line) and $MbTec^{32K}$ L396A (red, dashed line). ADP-Glo kinase assay; RLU (raw luminescence units).

Figure 3. MbTec adopts a compact conformation in solution.

A. Small-angle X-ray scattering (SAXS) curves of $MbTec^{FL}$ and $MbTec^{32K}$ in solution.

B. Pair distribution functions for $MbTec^{FL}$ and $MbTec^{32K}$.

C. Summary table of particle parameters derived from SAXS measurements

D. *Ab initio* molecular modeling of the molecular envelope of $MbTec^{FL}$. The structure of the Src SH2-SH3-kinase module (6F3F) was docked into the model using SUPCOMB (56).

E. *Ab initio* molecular modeling of the molecular envelope of $MbTec^{32K}$. The structure of the Src SH2-SH3-kinase module (6F3F) was superimposed with the model using SUPCOMB (56).

F. Pairwise HDX-MS analysis of $MbTec^{FL}$ compared to $MbTec^{32K}$. Significant differences in H/D exchange in $MbTec^{32K}$ are mapped onto an AlphaFold3 model of $MbTec^{32K}$ and are color coded according to the legend.

G. Pairwise HDX-MS analysis of $MbTec^{FL}$ compared to $MbTec^{PH}$. Significant differences in H/D exchange in $MbTec^{PH}$ are mapped onto B AlphaFold3 model of $MbTec^{PH}$ and are color coded according to the legend.

H. Sum of #D difference in deuterium incorporation for $MbTec^{32K}$ over the entire time course. Each point represents and individual peptide with significant changes shown in red (greater than 0.40 Da, 5% difference and two tailed t-test $p<0.01$ at any timepoint, n=3). Domain architecture is annotated above.

I. Sum of #D difference in deuterium incorporation for $MbTec^{PH}$ over the entire time course. Each point represents and individual peptide with significant changes shown in red (greater than 0.40 Da, 5% difference and two tailed t-test $p<0.01$ at any timepoint, n=3). Domain architecture is annotated above. The full deuterium exchange information for all peptides is included in the source data.

Figure 4. A gain-of-function mutation in the PH domain activates MbTec.

A. Second derivatives of the melting curves for $MbTec^{FL}$ (blue), $MbTec^{32K}$ (magenta). Solid lines: + 1mM ADP; dotted lines: -ADP. Inset: table of corresponding MbTec melting temperatures in the presence and absence of 1 mM ADP.

B. Radiometric autophosphorylation assays of $MbTec^{FL}$ (black, solid line) and $MbTec^{FL}$ E41K (orange, solid line), as well as $MbTec^{32K}$ L396A (red, dashed line) and $MbTec^{FL}$ E41K L396A (orange, dashed line).

C. Plasma membrane association of EGFP-MbTec^{FL} and mCherry-MbTec^{PH} in a representative NIH3T3 fibroblast following stimulation with PDGFαβ. Mask of filopodia-like membrane structures used for signal integration shown in magenta.

D. Bleaching-corrected, normalized mask intensity profiles of MbTec^{FL} (green) and MbTec^{PH} (red) in the region shown in panel C as a function of time, post-PDGFαβ stimulation.

E. Intramolecular PH-kinase interface in Akt1.

F. Sequence alignment of the activation loop-αF segment in the Tec kinases corresponding to the PH-kinase domain interface of Akt shown in panel E.

G. Melting temperatures of MbTec^{FL}(black), MbTec^{32K}(purple), MbTec^{FL} Y578A/R580A(orange) and MbTec^{FL} Y578D/R580E (red) with (filled circle) or without (empty circle) ADP.

Figure 5. MbTec is allosterically activated by PIP_3.

A. PIP_3-doped nanodiscs used to activate MbTec. MSP1D1 = membrane scaffold protein 1).

B. PIP_3-mediated activation of MbTec^{FL} (black, triangles) and MbTec^{FL} L396A (red, squares). Black, circles: MbTec^{FL} without PIP_3 nanodiscs.

C. Representative cartoons and autoradiograph for each construct. Note: the contrast has been artificially enhanced for the purposes of displaying the low basal autophosphorylation of MbTec^{FL} in the absence of PIP_3 nanodiscs.

D. Sequence conservation of the polyproline motif between Tec paralogs and over the course of vertebrate evolution. Representative human and turtle (*C. abingdonii*) sequences.

E. AlphaFold prediction of the intramolecular association of the Tec kinase polyproline motif with its SH3 domain.

F. Radiometric autophosphorylation time course of MbTec^{FL} (black) and MbTec^{FL} L396A (red), as well as MbTec^{FL} Gly_6 (orange) and MbTec^{FL} Gly_6 L396A (brown).

Figure 6. Model of PIP_3-mediated autoactivation of Tec family kinases.

Tec kinases adopt an autoinhibited conformation in the absence of an activating stimulus that is characterized by a discrete inhibitory interface between its PH and kinase domains (1). Upon ligand-mediated receptor activation and subsequent phosphorylation by non-RTKs, Tec is recruited by phospho-tyrosine motifs in the receptor tails and SH3 domain-containing adaptor proteins such as Grb2 (2) (for clarity, only the N-SH3 and SH2 domains of Grb2 (orange, dashed outline) are shown; the C-SH3 domain is reported to bind the PI3K p85 subunit (50)). Local concentration of Tec beneath the plasma membrane permits sampling of the membrane for PIP_3 (3), engagement of which is concomitant with disengagement of its PH and SH3 domains from its kinase domain. PIP_3 binding anchors Tec on the membrane and licenses its SH3 domain to compete with Grb2 for the polyproline motif in the PH-SH3 linker, thereby promoting allosteric activation of the kinase domain (4). Dimerization of Tec, driven by its local concentration on the membrane and possibly by reciprocal binding of the SH3 domain to the polyproline motif of a second Tec protomer, promotes activation loop autophosphorylation (5), thereby rendering Tec fully competent for downstream signaling. Upon loss of the PIP_3 signal, Tec is autoinhibited by its PH domain, thereby eliciting an acute termination of downstream signaling.

Figure 1. *Monosiga brevicollis* Tec binds and is stabilized by ADP.

A

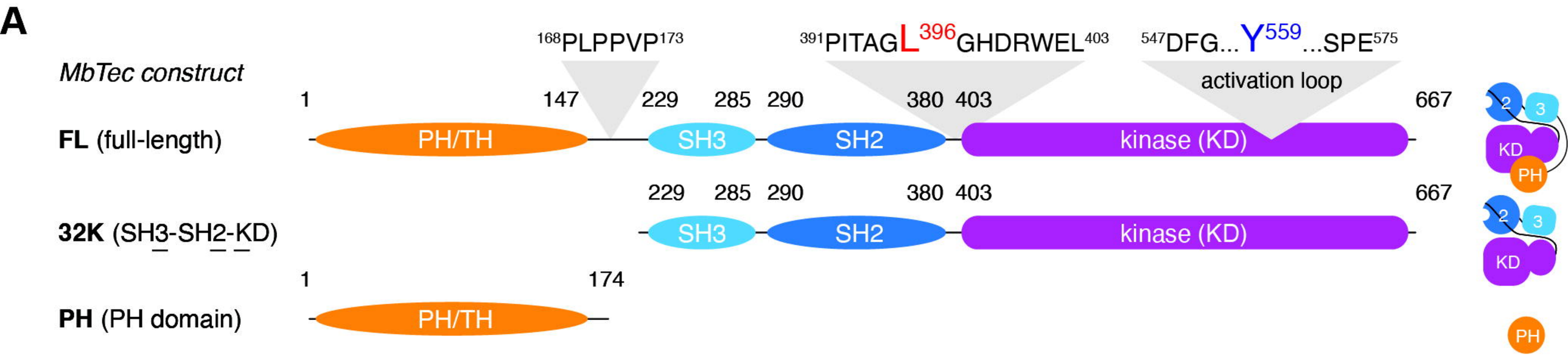

B

Hydrophobic stack conservation

Kinase	V3 (middle)	Trp (kinase N-lobe)	β2 (top) (kinase N-lobe)	β4 (bottom) (kinase N-lobe)
Btk	L390	W395	W421	Y461
Itk	L351	W356	W382	Y422
Tec	F358	W363	W389	Y429
MbTec	**L396**	**W401**	**Y427**	**L467**
Src	L255	W260	W286	Y326

C

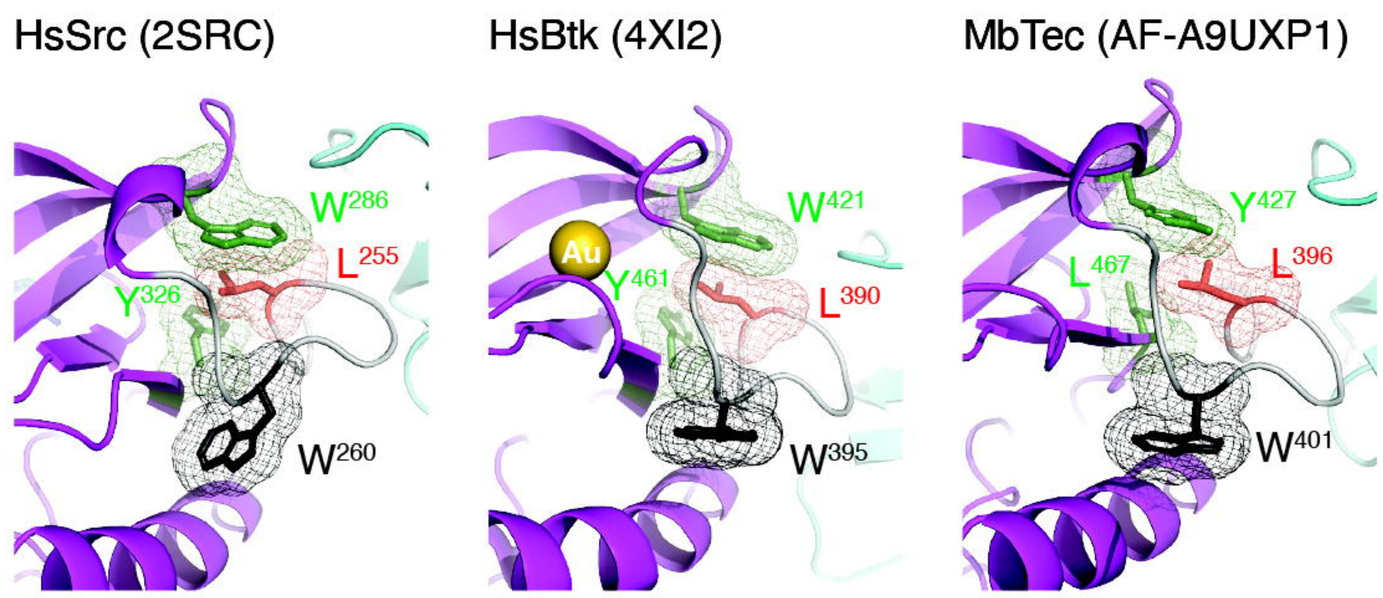

D

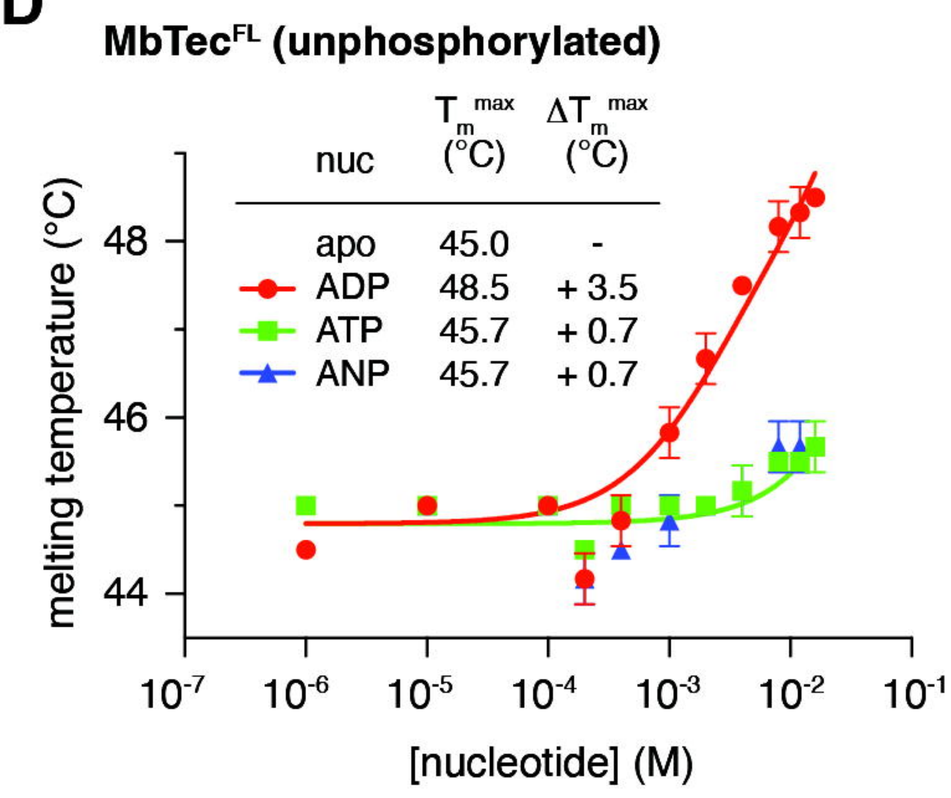

E

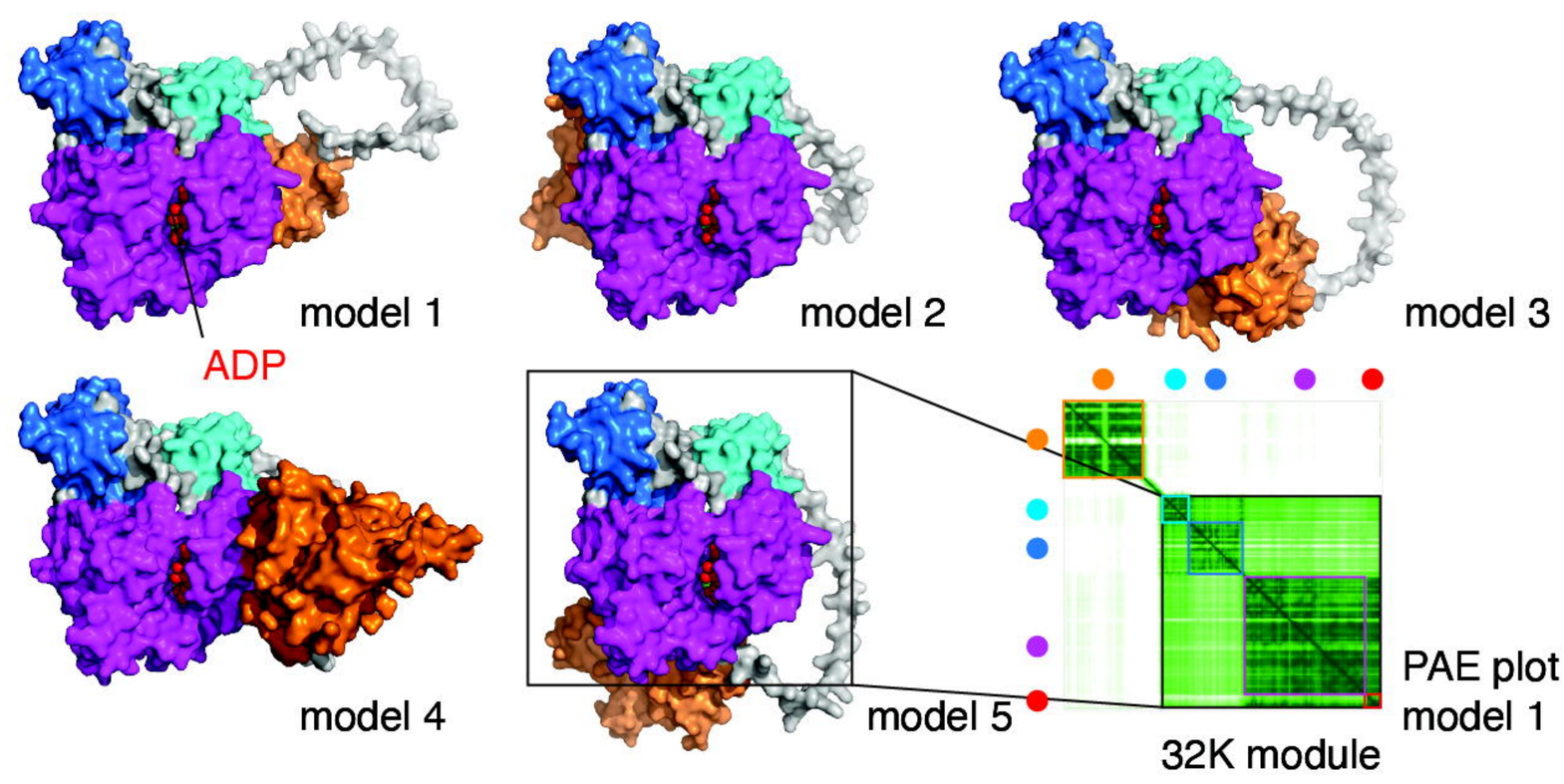

Figure 2. MbTec is autoinhibited by its PH domain.

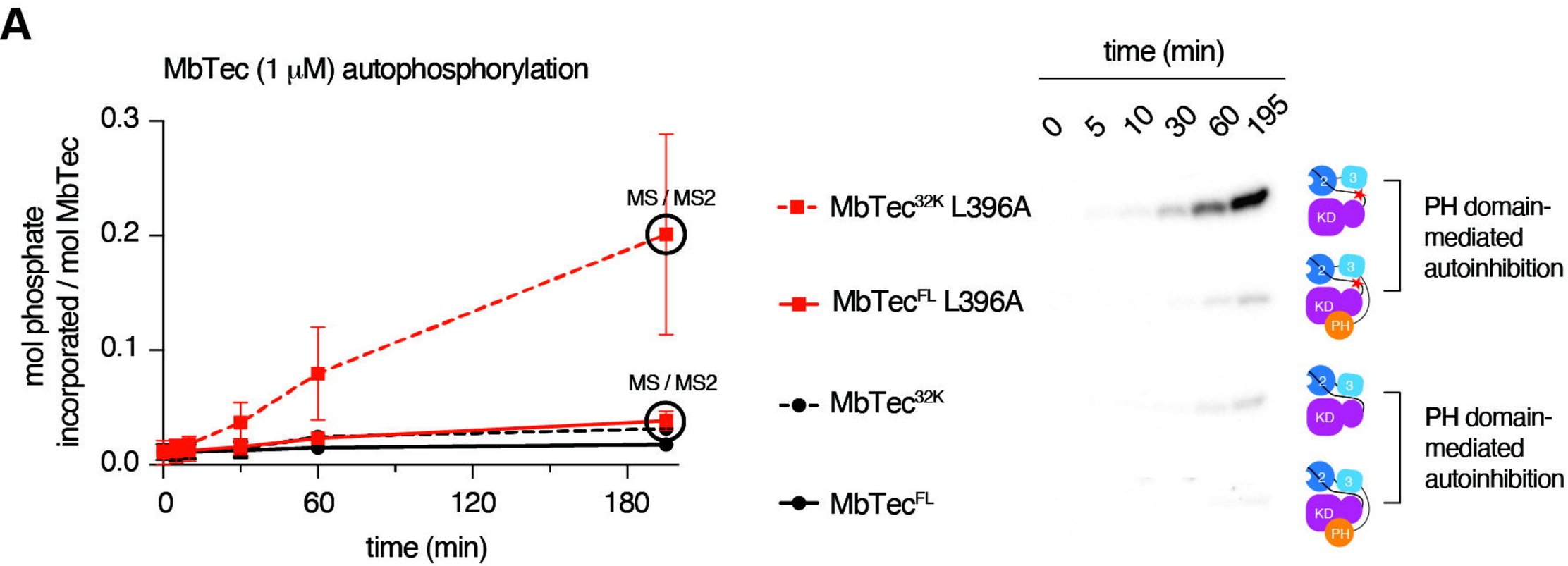

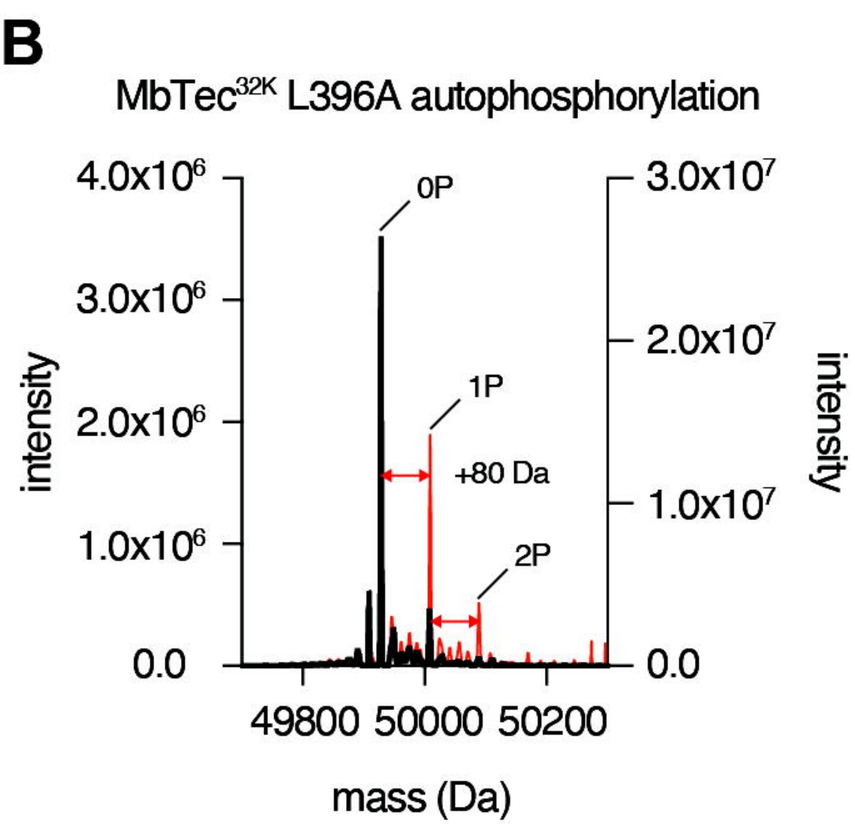

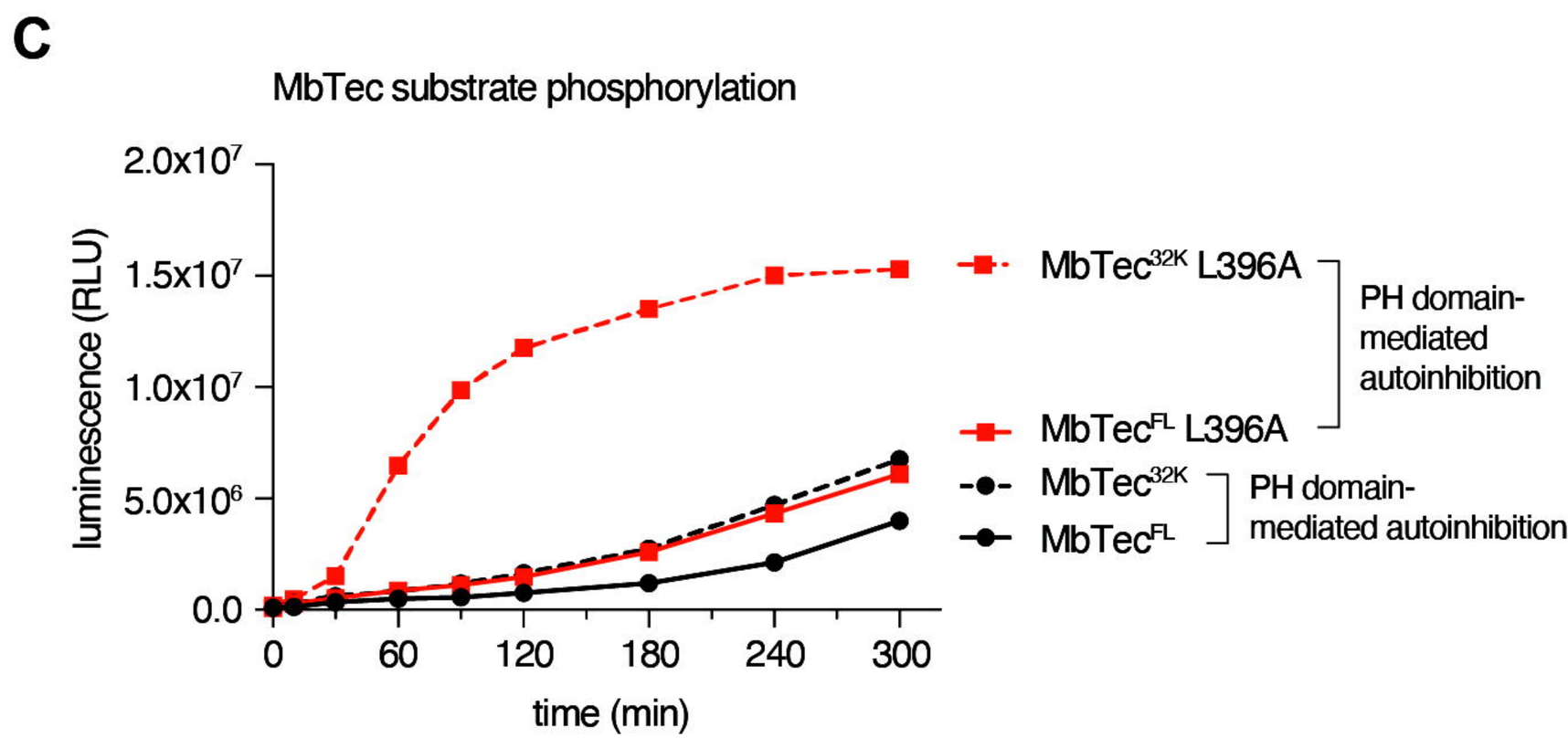

Figure 3. MbTec adopts a compact conformation in solution.

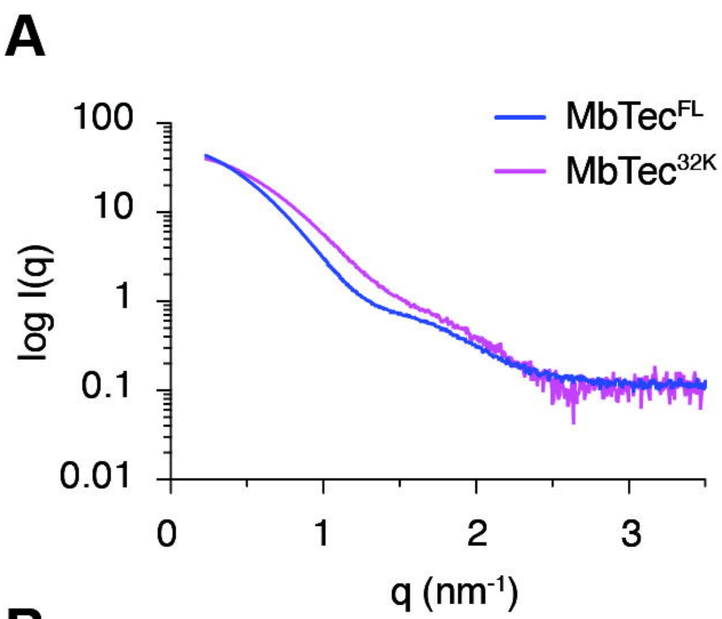

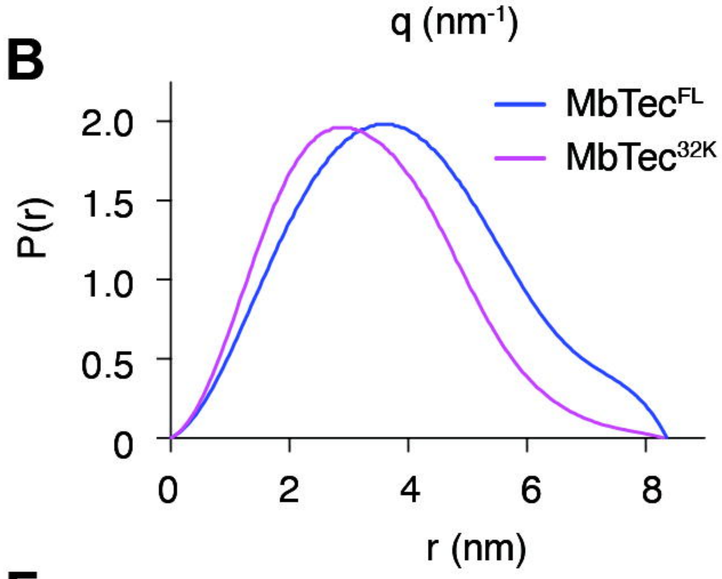

C

Protein	R_g (Guinier) (nm)	R_g (Gnom) (nm)	D_{max} (Gnom) (nm)	Mr est. (kDa)	Mr (actual) (kDa)
MbTec^FL	3.13 ± 0.01	3.04 ± 0.10	8.44	76.35	74.29
MbTec^32K	2.54 ± 0.00	2.55 ± 0.21	8.29	47.68	49.97

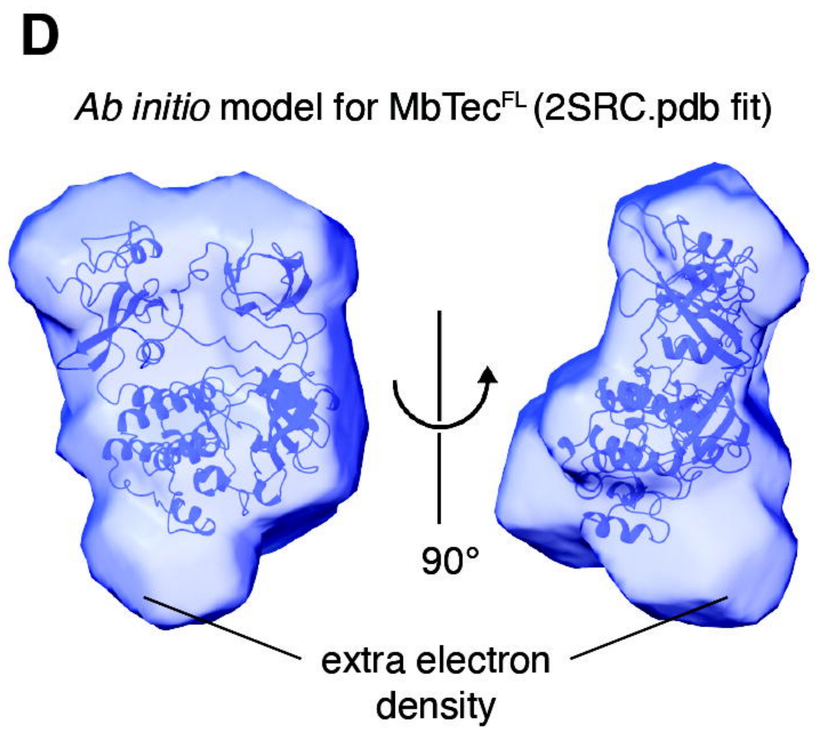

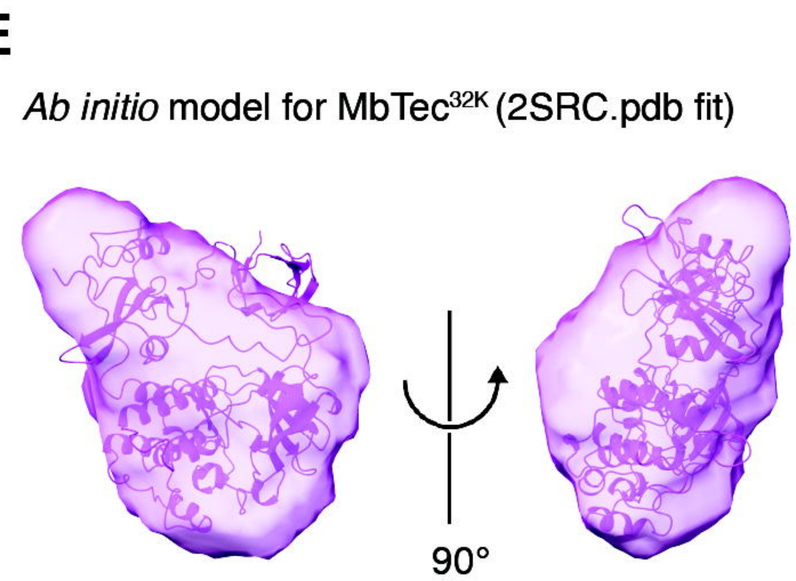

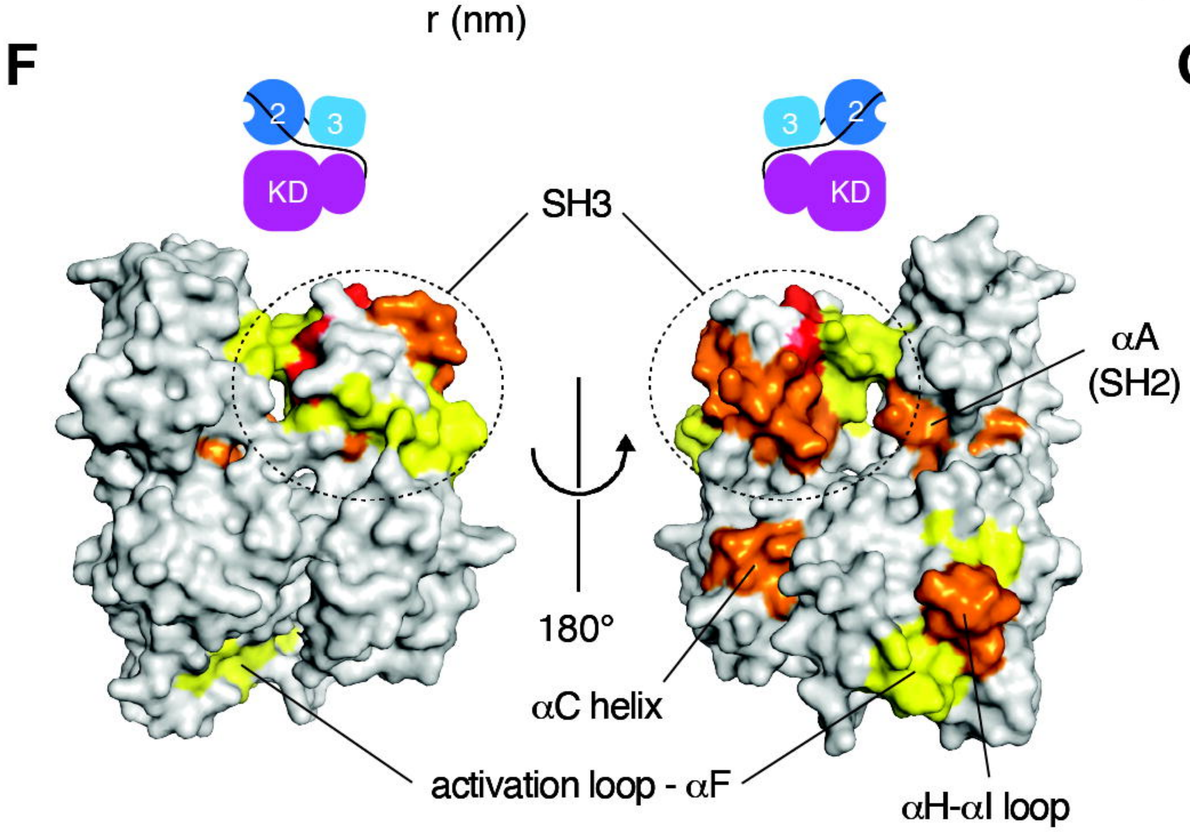

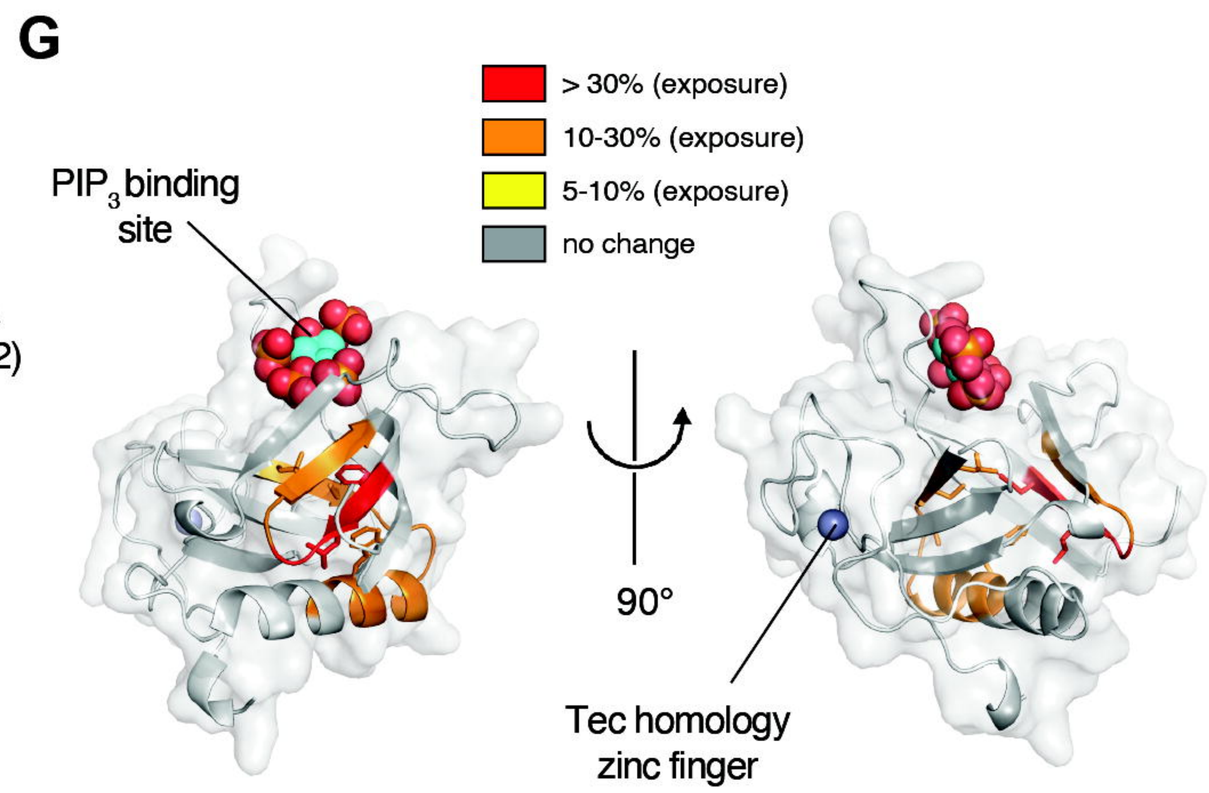

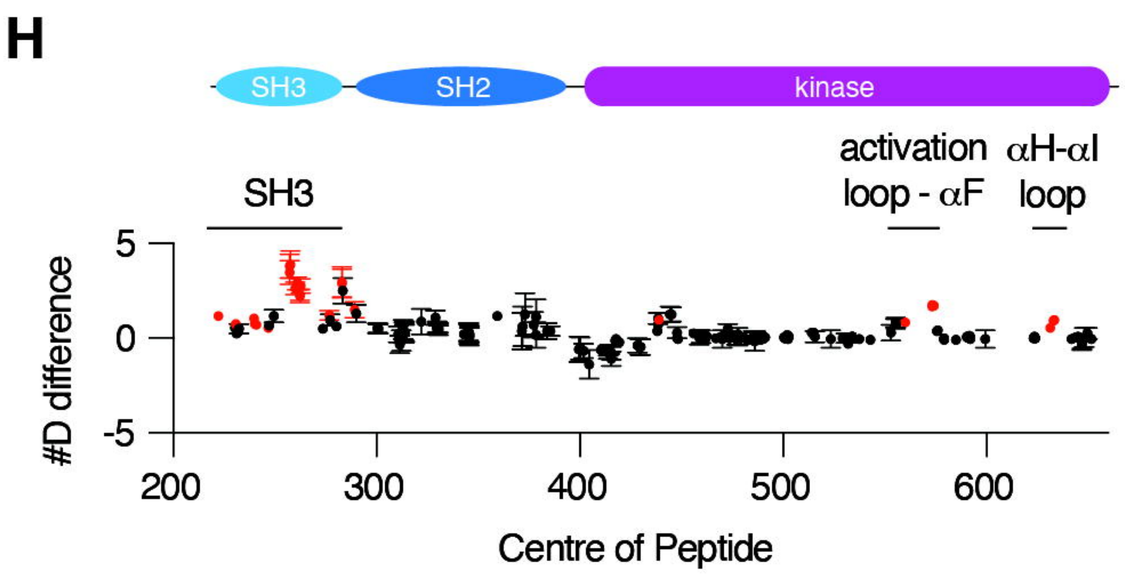

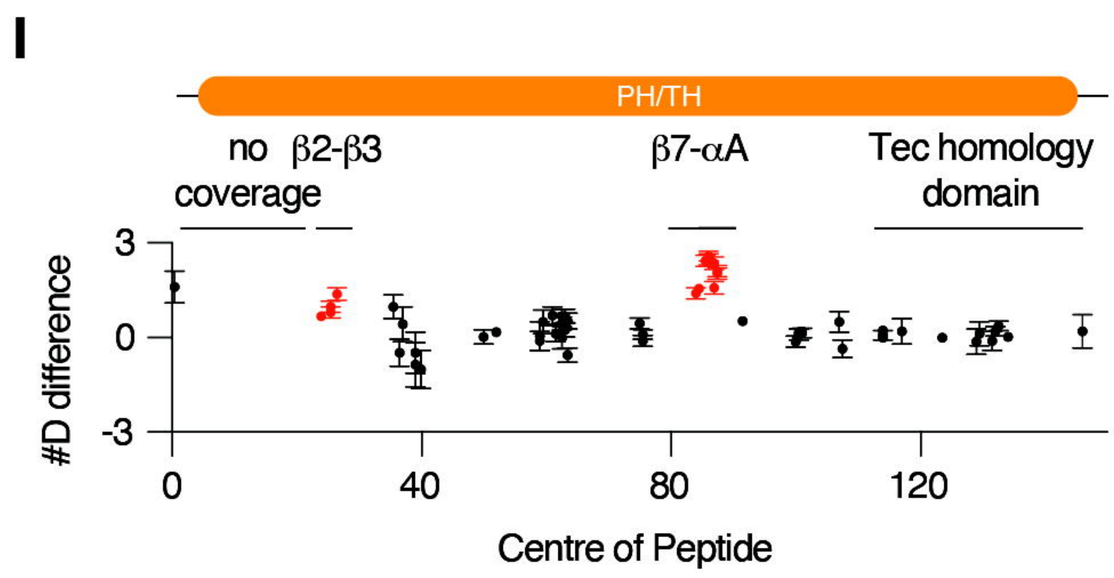

Figure 4. A gain-of function mutation in the PIP_3-binding pocket activates MbTec.

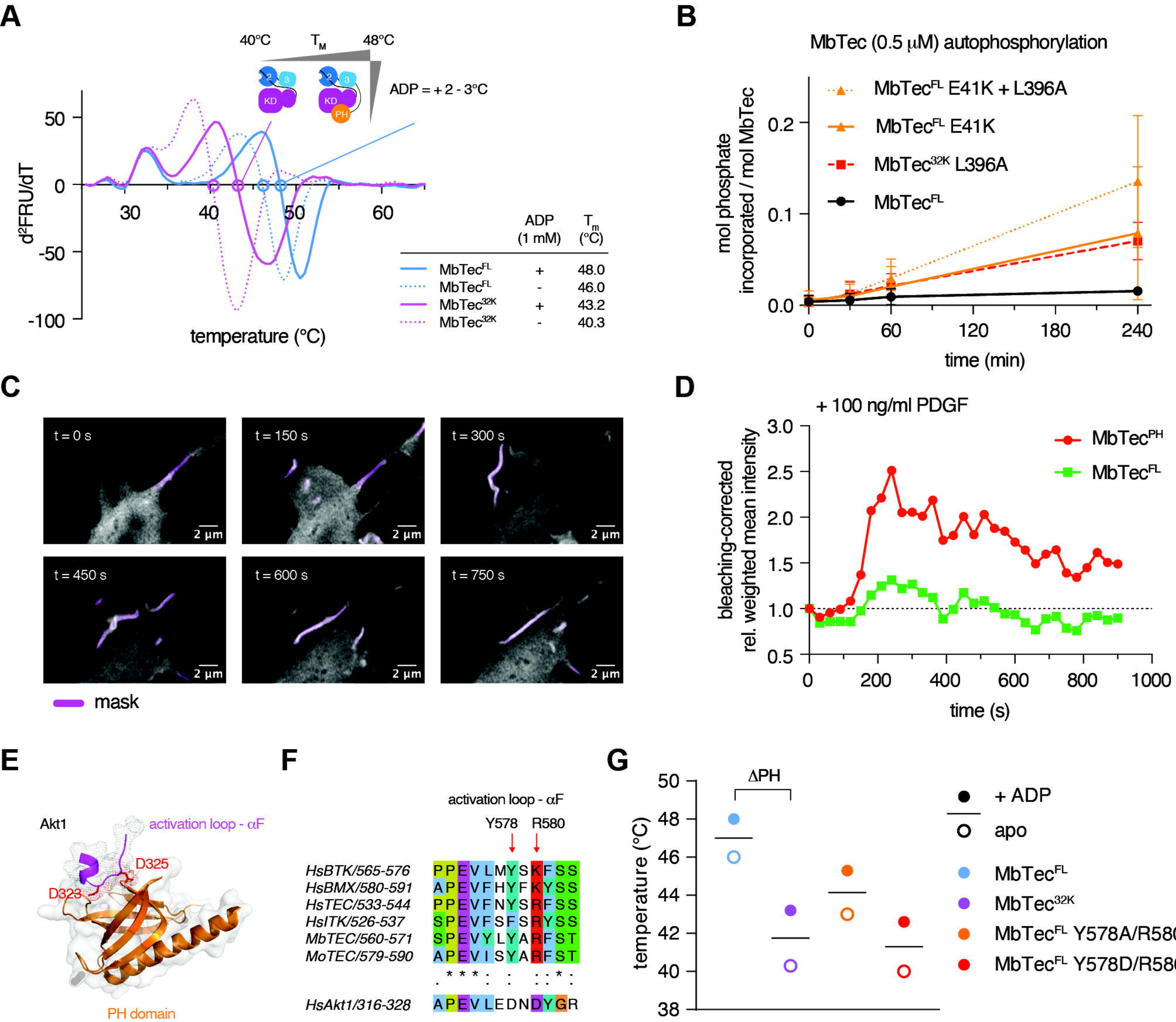

Figure 5. MbTec is allosterically activated by PIP_3.

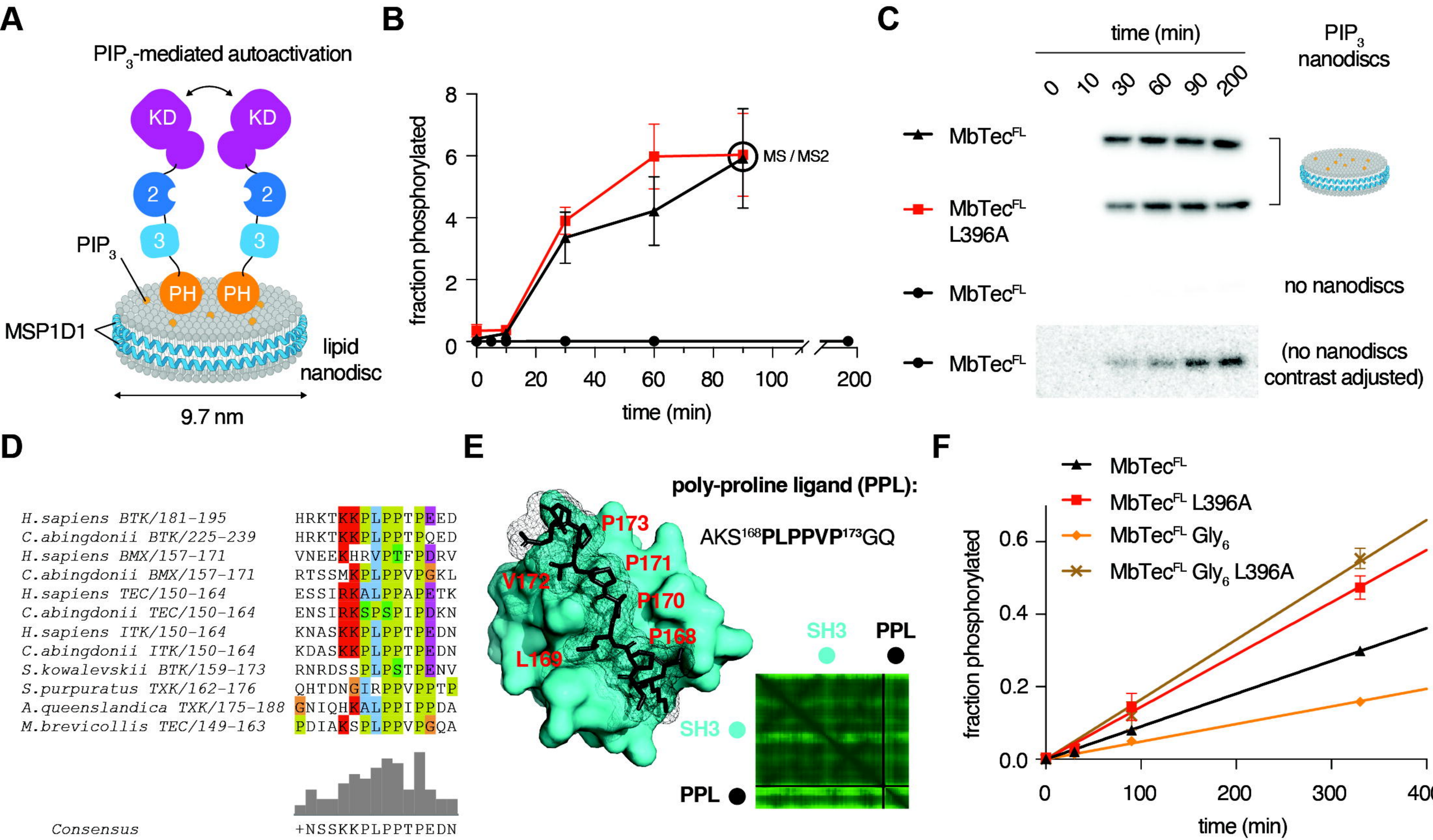

Figure 6. Model of PIP_3-mediated auto-activation of Tec family kinases.

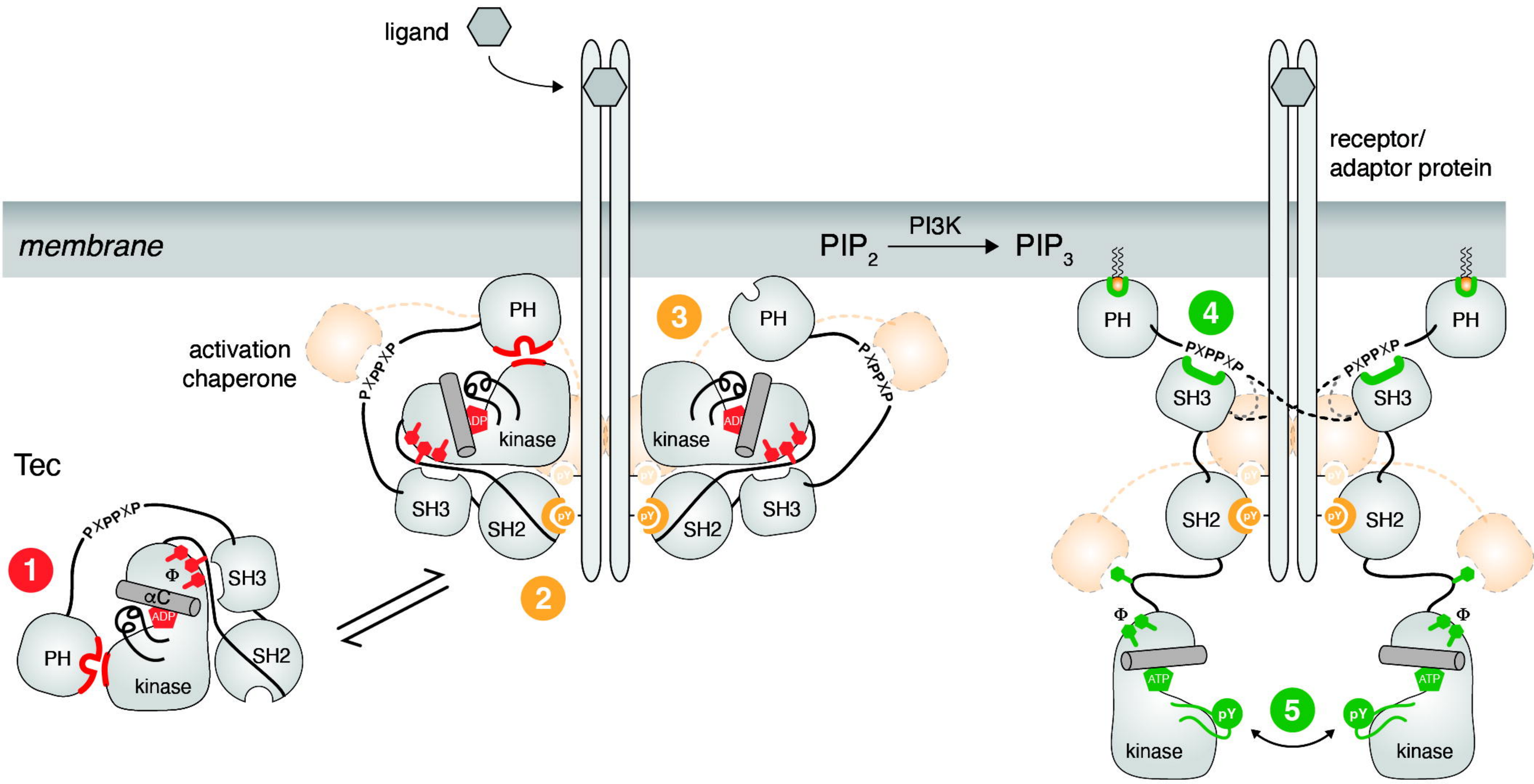

1 AUTOINHIBITION

2 RECRUITMENT

3 DYNAMIC SAMPLING

4 ALLOSTERIC ACTIVATION

5 AUTO-PHOSPHORYLATION